AD-A180 047 DYNAMIC CONTROL OF THE INPUT IMPEDANCE OF MICROSTRIP ELEMENTS USING REACTIVE LOADS(U) HOUSTON UNIV TX W F RICHARDS OCT 86 RADC-TR-86-115 F30602-81-C-0193 1/1

UNCLASSIFIED F/G 17/9 NL

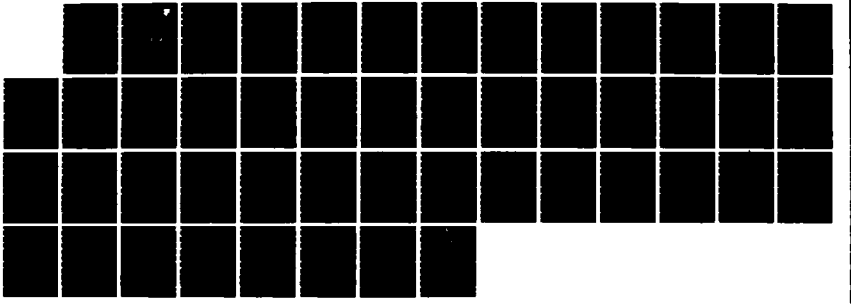

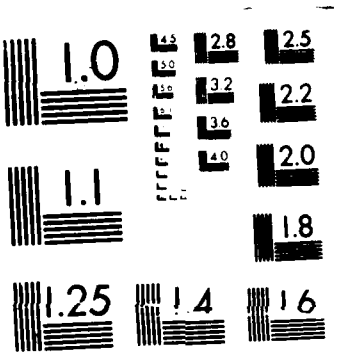

RADC-TR-86-115
Final Technical Report
October 1986

DYNAMIC CONTROL OF THE INPUT IMPEDANCE OF MICROSTRIP ELEMENTS USING REACTIVE LOADS

University of Houston

William F. Richards

APPROVED FOR PUBLIC RELEASE; DISTRIBUTION UNLIMITED

ROME AIR DEVELOPMENT CENTER
Air Force Systems Command
Griffiss Air Force Base, NY 13441-5700

This report has been reviewed by the RADC Public Affairs Office (PA) and is releasable to the National Technical Information Service (NTIS). At NTIS it will be releasable to the general public, including foreign nations.

RADC-TR-86-115 has been reviewed and is approved for publication.

APPROVED: John R Corneil

JOHN R. CORNEIL, 2LT, USAF
Project Engineer

APPROVED: Allan C. Schell

ALLAN C. SCHELL
Directorate of Electromagnetic Sciences

FOR THE COMMANDER: John A. Ritz

JOHN A. RITZ
Directorate of Plans & Programs

If your address has changed or if you wish to be removed from the RADC mailing list, or if the addressee is no longer employed by your organization, please notify RADC (EECS) Hanscom AFB MA 01731-5000. This will assist us in maintaining a current mailing list.

Do not return copies of this report unless contractual obligations or notices on a specific document requires that it be returned.

UNCLASSIFIED
SECURITY CLASSIFICATION OF THIS PAGE

REPORT DOCUMENTATION PAGE

1a. REPORT SECURITY CLASSIFICATION UNCLASSIFIED	1b. RESTRICTIVE MARKINGS N/A
2a. SECURITY CLASSIFICATION AUTHORITY N/A	3. DISTRIBUTION/AVAILABILITY OF REPORT Approved for public release; distribution unlimited.
2b. DECLASSIFICATION/DOWNGRADING SCHEDULE N/A	
4. PERFORMING ORGANIZATION REPORT NUMBER(S) N/A	5. MONITORING ORGANIZATION REPORT NUMBER(S) RADC-TR-86-115
6a. NAME OF PERFORMING ORGANIZATION University of Houston 6b. OFFICE SYMBOL (If applicable)	7a. NAME OF MONITORING ORGANIZATION Rome Air Development Center (EECS)
6c. ADDRESS (City, State, and ZIP Code) Houston TX 77004	7b. ADDRESS (City, State, and ZIP Code) Hanscom AFB MA 01731-5000
8a. NAME OF FUNDING/SPONSORING ORGANIZATION Rome Air Development Center 8b. OFFICE SYMBOL (If applicable) EECS	9. PROCUREMENT INSTRUMENT IDENTIFICATION NUMBER F30602-81-C-0193
8c. ADDRESS (City, State, and ZIP Code) Hanscom AFB MA 01731-5000	10. SOURCE OF FUNDING NUMBERS PROGRAM ELEMENT NO. 62702F; PROJECT NO. 4600; TASK NO. 15; WORK UNIT ACCESSION NO. P9

11. TITLE (Include Security Classification)
DYNAMIC CONTROL OF THE INPUT IMPEDANCE OF MICROSTRIP ELEMENTS USING REACTIVE LOADS

12. PERSONAL AUTHOR(S)
William F. Richards

13a. TYPE OF REPORT	13b. TIME COVERED	14. DATE OF REPORT (Year, Month, Day)	15. PAGE COUNT
Final	FROM Jan 85 TO Sep 85	October 1986	48

16. SUPPLEMENTARY NOTATION
N/A

17. COSATI CODES			18. SUBJECT TERMS (Continue on reverse if necessary and identify by block number)
FIELD	GROUP	SUB-GROUP	Dynamic Impedance Tuning Microstrip Elements Phased Arrays
17	09		
20	14		

19. ABSTRACT (Continue on reverse if necessary and identify by block number)

Great effort has been expended to develop MMIC modules for active aperture phased array radar antennas. The motivation for this work is to reduce the size, complexity and cost of phased arrays for space, airborne and ground based applications. Unfortunately, a large change in element input impedance occurs when the array is scanned. To isolate the module from this change, a ferrite circulator is inserted between the module and the antenna element. The insertion of the circulator is in direct conflict with the concept of MMIC and increases the module cost because it requires the introduction of circuit elements as a separate step in the production process. This final report is a theoretical and experimental evaluation of dynamically tuning patch radiators. The results of this study show that it is possible to change the input impedance of a microstrip element over a wide range without affecting its resonant frequency or co-planar pattern by moving short circuits from one point to another. Having this capability may alleviate the need for the ferrite circulators, thus reducing the size, complexity and cost of phased array antennas.

20. DISTRIBUTION/AVAILABILITY OF ABSTRACT ☒ UNCLASSIFIED/UNLIMITED ☐ SAME AS RPT ☐ DTIC USERS	21. ABSTRACT SECURITY CLASSIFICATION UNCLASSIFIED
22a. NAME OF RESPONSIBLE INDIVIDUAL John R. Corneil, 2Lt, USAF	22b. TELEPHONE (Include Area Code) (617) 377-2059 22c. OFFICE SYMBOL RADC (EECS)

DD FORM 1473, 84 MAR 83 APR edition may be used until exhausted. All other editions are obsolete.

SECURITY CLASSIFICATION OF THIS PAGE
UNCLASSIFIED

17. COSATI CODES (Continued)

Field	Group
01	03

Contents

List of Figures

1 Introduction

During the contract period, we conducted a study of the feasibility of controlling the input impedance of a microstrip element by dynamically changing its loading. The motivation for this work is the possibility of using such elements in a scanned array. By changing the loading of the elements appropriately, one could alter the active array impedance of the elements perhaps compensating to some degree for the onset of scan blindness. While this report did not establish or refute the feasibility of the *ultimate* application, it definitely establishes the feasibility of controlling input impedance of a single element by using PIN shorting diodes.

The basic theory of loaded elements is briefly reviewed in the next section. Those features of the theory pertinent to the current application are discussed in more detail in the third section. The theoretical results and the corresponding experimental results are also presented in this section. Conclusions and suggested future research are given in the last section. Additional details of the analytical methods used can be found in Appendix A. Many of these theoretical results were just recently developed and are not presented elsewhere in the open literature. In particular, the extraction of quasistatic terms, detailed in Appendix A, makes the interactive design of these types of loaded elements feasible. This is because the determination of the resonant frequency of a loaded element is a non-linear problem requiring the iterative solution of the characteristic equation. Efficiency in computation, therefore, is critical—and the quasistatic analysis presented is highly efficient.

2 Theory of Loaded Microstrip Antennas

A brief overview of the theory of loaded microstrip antennas is presented in this section. A more detailed discussion can be found in [1].

For design purposes, one needs a simple theory which sheds light on the physical mechanisms of the microstrip antenna. Even if the theory is not the most quantitatively accurate, it is still vital to understand its physics if one is going to do creative things with the element. One theory that has proven to be physically illuminating, and relatively accurate as well, is the cavity-model analysis. It is this analysis that is used as a basis for design of loaded microstrip elements.

A typical microstrip element is illustrated in Fig. 1. The fundamental assumption made in cavity-model analysis is that the *distribution* of the field between the patch and the ground plane is approximately the same as that resulting in a cavity formed by closing the edge of the patch to the ground plane as illustrated in Fig. 2. The *amplitude* of the field distribution in the antenna and in the cavity are different. The method of determining this amplitude will be discussed later. ***For the purpose of determining the resonant frequency of the loaded element, the antenna will be assumed to be the same as the corresponding cavity.***

2.1 Unloaded microstrip cavity

In order to analyze the loaded cavity ultimately of interest in this report, one must first understand the analysis of an unloaded cavity. Suppose one impresses a uniform, unit, vertical, filamentary electric current as illustrated in Fig. 2. The resulting cavity electric field will be vertically directed. Let the vertically directed electric field produced be denoted by $G(\boldsymbol{\rho}|\boldsymbol{\rho}')$, where $\boldsymbol{\rho}$ is the two-dimensional position vector locating the

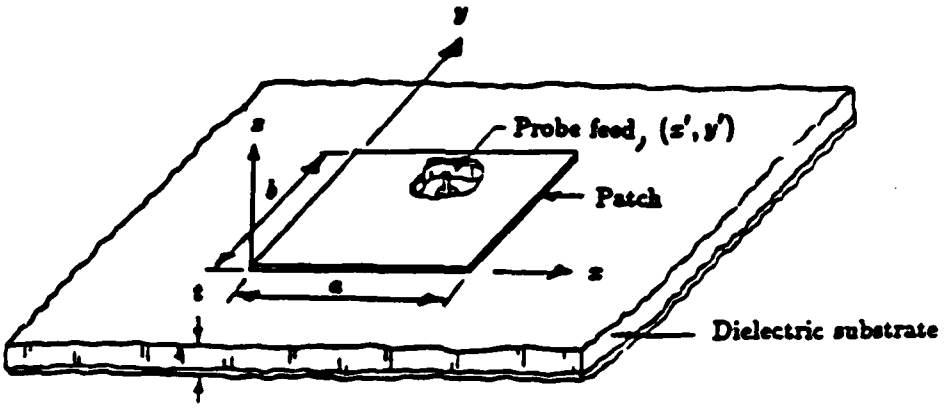

Figure 1: Illustration of a typical, rectangular patch element showing dimensional parameters and coordinate system.

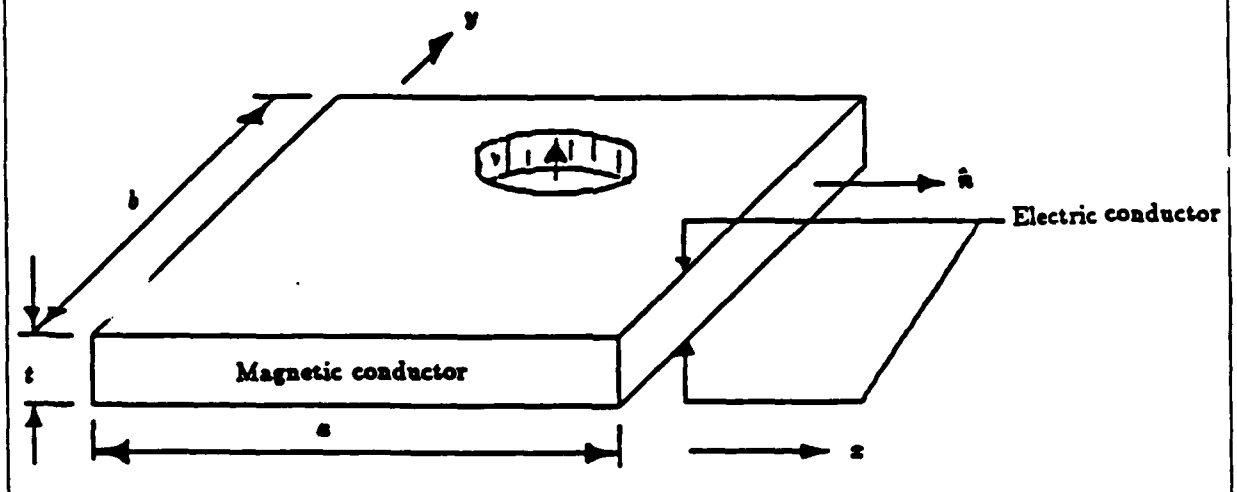

Figure 2: The cavity model of a microstrip element.

observation point within the cavity, and $\mathbf{r}'$ is the corresponding position vector locating the source current. Since this field is produced by a concentrated unit source, the field $G(\mathbf{r}|\mathbf{r}')$ can be thought of as a Green's function. The boundary-value problem that this Green's function satisfies is

$$(\nabla^2 + k^2)G(\mathbf{r}|\mathbf{r}') = j\omega\mu\delta(\mathbf{r} - \mathbf{r}'), \quad \mathbf{r} \in S,$$

$$\nabla G(\mathbf{r}|\mathbf{r}') \cdot \hat{\mathbf{n}} = 0, \quad \mathbf{r} \in \partial S,$$

where S denotes the set of points on the patch, ∂S denotes the boundary of S, and $\hat{\mathbf{n}}$ is the outward-pointing unit normal on ∂S. The solution of this boundary-value problem is

$$G(\mathbf{r}|\mathbf{r}') = j\omega\mu \sum_{A} \frac{\psi_{mn}(\mathbf{r})\psi_{mn}(\mathbf{r}')}{k^2 - k_{mn}^2}, \tag{1}$$

where A is the set of all pairs of non-negative integers, (m, n), and $\psi_{mn}(\mathbf{r})$ is the mn^{th} mode of the cavity satisfying

$$\nabla^2\psi_{mn}(\mathbf{r}) = -k_{mn}^2\psi_{mn}(\mathbf{r}), \quad \mathbf{r} \in S,$$

$$\nabla\psi_{mn}(\mathbf{r}) \cdot \hat{\mathbf{n}} = 0, \quad \mathbf{r} \in \partial S.$$

The series for $G(\mathbf{r}|\mathbf{r}')$ diverges as $\mathbf{r} \rightarrow \mathbf{r}'$. This is because the inductive reactance associated with a filament is infinite. In order to obtain the input reactance of an *actual* feed, one must integrate this Green's function over the actual feed current distribution. This integration is typically a surface integral over the outer periphery of the feed structure. For the purposes of this report, it is assumed that all source and load currents are distributed uniformly on a circular cylinder of diameter d. The "location" of the source or feed is the center of the cylinder's cross section. The input impedance of the element can be found by placing the observation point at the center of the cross section of the feed, and by integrating the Green's function over the surface current. When this is done, one obtains an input reactance of

$$X_{\text{in}} = X_{\text{f}} + X_{\text{r}},$$

where

$$X_{\text{r}} = -j\omega\mu t \frac{\psi_{mn}(\mathbf{r})\psi_{mn}(\mathbf{r}')}{k^2 - k_{mn}^2}$$

is the *resonant* reactance and X_{f} is the *feed* reactance. The parameter t is the thickness of the dielectric under the patch. The pair (m, n) represents the indices of the "resonant mode." For the case of loaded microstrip elements, the resonant mode selected for determining X_{r} is the mode of the *unloaded cavity* that resonates at a frequency closest to that of the mode of interest in the *loaded cavity*. The feed reactance is the contribution to the total reactance from all of the non-resonant modes, principally, the higher-order modes of the element. The feed reactance is typically inductive and varies slowly with frequency. Of course, if the frequency varies too far from the resonant frequency associated with the indices (m, n), the feed reactance will contain resonant components as well. The circuit model associated with this is illustrated in Fig. 3. The resonant mode of the *loaded* element can be conveniently expressed in terms of the modes of the corresponding *unloaded* cavity as described below.

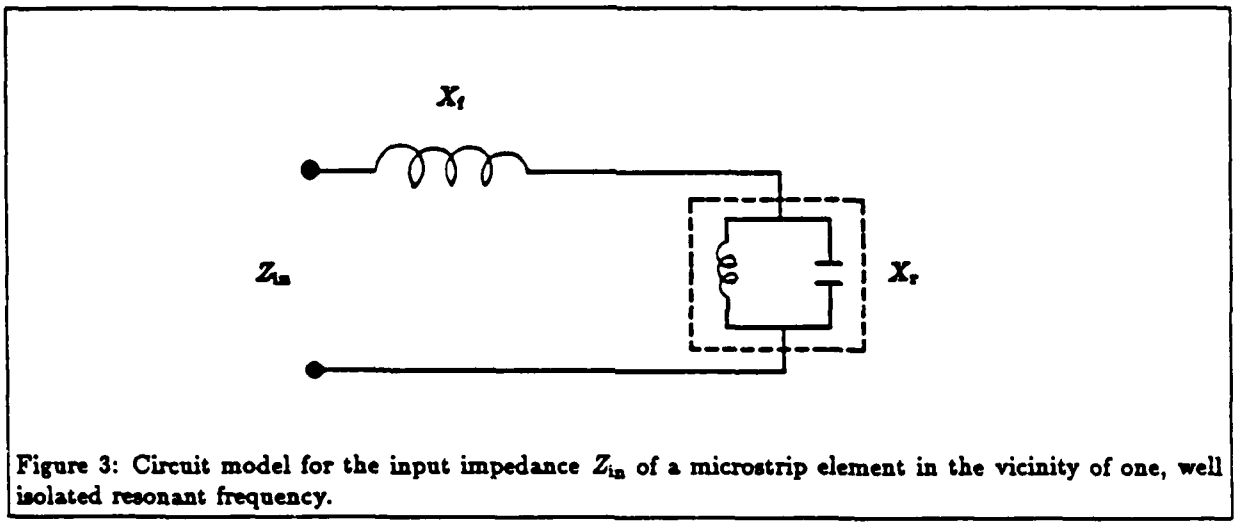

Figure 3: Circuit model for the input impedance Z_{in} of a microstrip element in the vicinity of one, well isolated resonant frequency.

2.2 Loaded microstrip cavity

The resonant frequency of a loaded cavity is that frequency at which the cavity can support a source-free cavity mode. At that frequency, in general, a non-sero current will flow through the multiple loads of the cavity even though no source current is applied. A non-separable loaded cavity can be converted to a separable cavity by using the equivalence principle. If the loads are removed and equivalent electric and magnetic currents are impressed on the surface bounding the now absent loads, then the field produced within the now unloaded cavity is the same as that of the original loaded cavity. It turns out that the magnetic currents called for by the equivalence principle are typically negligible [1]. The *total* electric current impressed at the location of each load is the total source-free load current that flows through the load. The unloaded cavity, in contrast to the loaded cavity is now *driven* by the load currents, although the load currents are, as yet, undetermined. To understand how to determine the load currents and to better understand the role played by load location, consider first an element loaded by just a single load.

2.2.1 Single load

Suppose that the load has a reactance of X_L. Then the network model of the undriven loaded cavity is that illustrated in Fig. 4. A source-free mode is desired. That is, one seeks to produce a non-sero load current with no source. This is only possible if the network is resonant. Summing the voltage around the closed loop yields the condition for resonance,

$$X_r + X_f + X_L = 0,$$

or

$$X_r = -X_f - X_L.$$

To best interpret this characteristic equation, consider the simple and very practical case of a short-circuit load. In this case, $X_L = 0$. Figure 5(a) contains a plot of X_r *versus* frequency for a rectangular

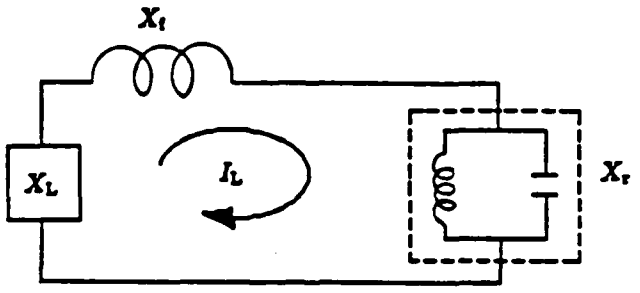

Figure 4: Circuit model of a cavity loaded with a single load reactance of X_L.

microstrip antenna for three different load locations as illustrated in Fig. 5(b). It also contains plots of the negative of the feed reactance corresponding to each feed location. The intersection of corresponding curves is the resonant frequency of the shorted microstrip element.

The resonant mode in Fig. 5 is the $(0,1)$ mode, the mode most commonly used in microstrip elements. For a rectangular element of dimensions $a \times b$, the normalized voltage distribution at observation point (x, y) for the $(0,1)$ mode is

$$v(x,y) = \cos\left(\frac{\pi y}{b}\right).$$

This is zero on the center line, $y = b/2$, of the patch. Such a line of zero field is called a nodal line. A point at which the voltage is stationary is called an anti-nodal point. All points on the long edges of the patch illustrated in Fig. 5 are anti-nodal points. When the load current is impressed near a nodal line, the resonant reactance curve becomes very skinny as illustrated by case 3 in Fig. 5(a). In contrast, when the load current is impressed near an anti-nodal point such as in case 1 of Fig. 5(b), then the X_r curve becomes fat. Since the voltage is stationary near an anti-nodal point, the X_r curve does not change much as one moves the load in the vicinity of the anti-nodal point. Thus the curve illustrated in case 2 of Fig. 5(a) is not much different from the case 1 curve.

This variation of the X_r curve would predict that the resonant frequency should monotonically increase as the short is moved from the nodal line to an anti-nodal point *if the feed reactance were to remain constant.* However, as shown in [2], the feed reactance is anything but constant with the feed position. In fact, the feed reactance increases very rapidly as the feed point approaches the edge of the patch. If the edge is an anti-node, then the X_r curve does not change much as the load is moved toward the edge, but the $-X_f$ curve is moving rapidly downward in the graph in Fig. 5 so that the resonant frequency of the shorted element decreases for loads near the edge. This makes sense because as the feed reactance increases, it becomes more like an open circuit and thus its loading effect is reduced. A typical theoretical frequency *versus* short position variation is illustrated in Fig. 6. The actual measured variation of resonant frequency with the

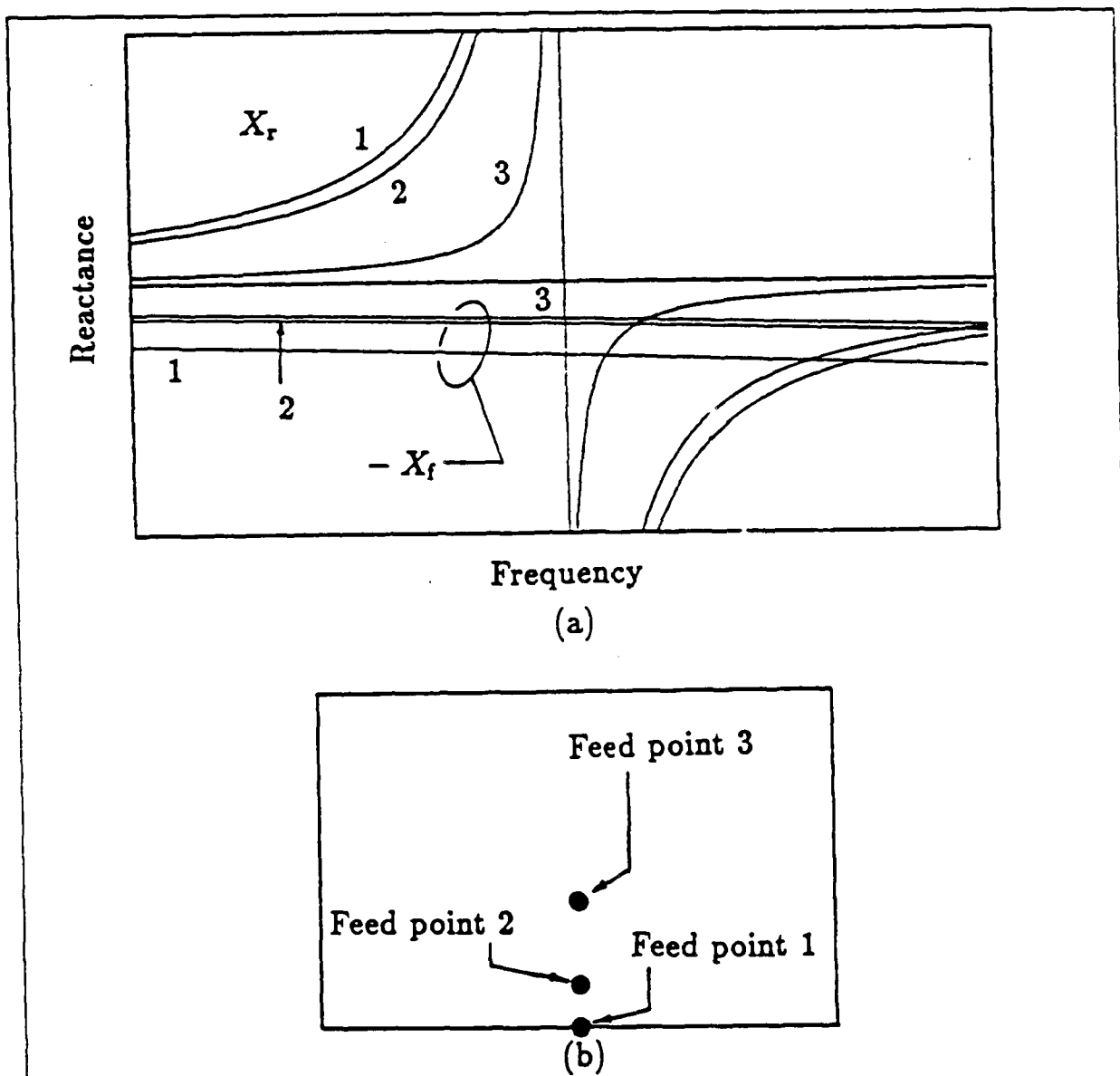

Figure 5: (a) *Illustration of* X_r *and* $-X_f$ *versus* frequency for the three feed locations illustrated in (b). (b) Rectangular patch showing three different feed locations.

location of the short agrees well with the predicted results. The location of the shorting pin is indicated by the normalized shorting pin location defined as

$$s = \frac{2}{b}\left(y' - \frac{b}{2}\right).$$

If one uses other types of load reactances, the resonant frequency of the loaded element will be modified although the effect of the feed reactance is always present. Examples of other applications of loaded microstrip elements can be found in [3], [4]. For the current application of controlling input impedance, one should *not* use just a single load. The reason why will be explained in the next section.

2.2.2 Multiple loads

For multiple loads, one cannot use the simple graphical picture presented above for predicting the behavior of a multiple-loaded element although the principles learned from this picture still apply.[1] For multiple loads, the characteristic equation is

$$\begin{vmatrix} Z_{11} + Z_L^{(1)} & Z_{12} & \cdots & Z_{1N} \\ Z_{12} & Z_{22} + Z_L^{(2)} & \cdots & Z_{2N} \\ \vdots & \vdots & & \vdots \\ Z_{1N} & Z_{2N} & \cdots & Z_{NN} + Z_L^{(N)} \end{vmatrix} = 0, \tag{2}$$

where Z_{ij} is the z-parameter between the i^{th} and j^{th} port of a multiple-port microstrip cavity, and $Z_L^{(i)}$ is the load impedance connected to the i^{th} port. The z-parameters can be computed using equation (1) as modified by integrating over the feed current distribution.[2] Once the resonant frequency is determined, the next step is to compute the modal field distribution of the loaded-cavity resonant mode.

To determine the field distribution of the resonant mode, one must first assume a unit (or any other non-zero current) at one of the ports and then compute the resulting currents at the remaining loads. Let $\mathbf{Z}_s$ be a submatrix excluding the first row and column of the matrix in equation (2). Let $\mathbf{Z}_{1s}$ be the first column of the matrix in equation (2), excluding the first row. Let $\mathbf{I}$ be the column matrix of port currents excluding the current in port 1,

$$\mathbf{I} = \begin{bmatrix} I_2 \\ I_3 \\ \vdots \\ I_N \end{bmatrix}.$$

Then, if the load current in port 1 is $I_1 = 1$, the currents in the remaining ports are

$$\mathbf{I} = -\mathbf{Z}_s^{-1}\mathbf{Z}_{1s}.$$

[1] Actually, one could, in principle, apply the graphical analysis sequentially. That is, first find the effect of a single load. Then create a new graph in which X_r is the resonant reactance and X_f is the feed reactance of the *singly-loaded patch*. From these, the resonant frequency of the doubly-loaded element could be constructed.

[2] There is more to the computation than what has been outlined here. A very *efficient* analysis has been devised for computing the z-parameters in which the series is highly accelerated. The details of this are included in Appendix A.

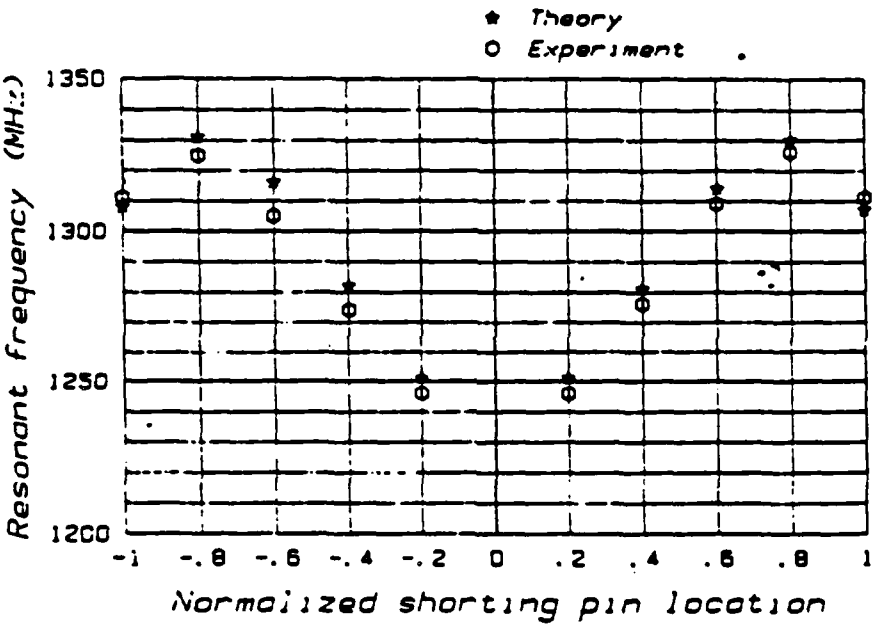

Figure 6: Theoretical and experimental resonant frequencies of a shorted microstrip patch antenna versus shorting pin location.

The resulting field distribution is

$$\Psi(\mathbf{r}) = j\omega\mu \sum_{A} \sum_{\ell=1}^{N} I_\ell \frac{\psi_{mn}(\mathbf{r})\psi_{mn}(\mathbf{r}_\ell)}{k^2 - k_{mn}^2}, \tag{3}$$

where $\psi_{mn}(\mathbf{r})$ and k_{mn} are the modal fields and corresponding resonant wavenumbers in the *unloaded* cavity. Strictly speaking, this expression is only valid for observation points $\mathbf{r}$ outside of the load regions. That is, if the diameter of the i^{th} load is d_i, then $|\mathbf{r} - \mathbf{r}_i|$ must be larger than $d_i/2$.

The input impedance of the loaded element is computed by analyzing the cavity with the actual dielectric replaced with an artificially lossy dielectric—one whose losses account for the radiative and ohmic losses of the original microstrip antenna. The *effective loss tangent* of this dielectric is $\delta_{\text{eff}} = 1/Q$ where Q is the quality factor of the antenna. It is given by

$$Q = \left(\frac{1}{Q_{\text{rad}}} + \frac{1}{Q_{\text{sw}}} + \frac{1}{Q_{\text{m}}} + \frac{1}{Q_{\text{d}}} \right)^{-1},$$

where Q_{rad} is the radiative quality factor, Q_{sw} is the quality factor associated with the surface wave, Q_{m} is the quality factor associated with metal heating loss, and Q_{d} is the dielectric quality factor. These are given by

$$Q_{\text{rad}} = \frac{2\omega W_E}{P_{\text{rad}}},$$

$$Q_{\text{sw}} = \frac{2\omega W_E}{P_{\text{sw}}},$$

$$Q_{\text{m}} = \frac{t}{\Delta},$$

$$Q_{\text{d}} = \frac{1}{\delta},$$

where P_{rad} is the time-averaged power radiated by the antenna, P_{sw} is the time-averaged power carried away by the surface wave, Δ is the skin depth in the metal cladding, δ is the loss tangent in the *actual* dielectric, and W_E is the average energy stored in the electric field at the resonant frequency of the cavity

The parameters in the expressions for the quality factors would appear to depend on the field under the patch. Actually, the quality factors depend only on the *distribution* of the mode for which the quality factors are being computed. The field could be multiplied by any arbitrary constant without affecting the quality factor. At the resonant frequency of the $\Psi(\mathbf{r})$ of the loaded element, the field is strongly dominated by $\Psi(\mathbf{r})$ itself. Thus, one can obtain an approximation for the quality factors by assuming the field distribution below the patch is $\Psi(\mathbf{r})$, with the contributions of the other non-resonant modes of the loaded patch ignored .

The radiated field can be computed under the following approximation. The ground plane and the dielectric are ignored, and a magnetic current filament is impressed in the presence of the ground plane. The magnetic current flows around the edge of the patch and is equal to the voltage between the patch and the ground plane. The surface wave can be determined by allowing this same magnetic current filament to

act in the presence of a grounded dielectric slab, although for sufficiently thin elements, the power carried in the surface wave is negligible. The magnetic current is actually sampled at discrete points and linearly interpolated between the sample points.[3] The radiated field is computed analytically and the associated radiated power is determined by numerical quadrature.

The electric stored energy is computed by integrating the square of the electric field. That is,

$$W_E = \frac{1}{2} t\epsilon \iint_S |E|^2 dS \approx \frac{1}{2} t\epsilon \iint_S |\Psi(r)|^2 \, dS. \tag{4}$$

The singularities at the load locations in equation (3) are logarithmic; their squares are integrable. As a result, equation (3) can be used for $t|E|$ with little error. Since the modes of the unloaded cavity are orthonormal, the double integration above reduces to[4]

$$\omega W_E = \frac{1}{2} t\epsilon_r \mu_r^2 k_0^3 \eta_0 \sum_{\ell=0}^{N} \sum_{i=0}^{N} I_\ell I_i \sum_A \frac{\psi_{mn}(r_i)\psi_{mn}(r_\ell)}{(k^2 - k_{mn}^2)^2}.$$

Once the quality factor of the loaded element is determined, then its input impedance can be computed.

2.3 Input Impedance

Assume that one more port is added to the antenna, the $(N+1)^{st}$ port. The circuit model as seen from the $(N+1)^{st}$ port for the loaded *cavity* is illustrated in Fig. 7. The circuit model of the *antenna* is shown in Fig. 8. The input admittance of the lossy tank circuit *only* is

$$\begin{aligned} Y_r &= G\left[1 + jQ\left(\left(\frac{\omega}{\omega_0}\right)^2 - 1\right)\right] \\ &\approx G\left[1 + j2Q\left(\frac{\omega}{\omega_0} - 1\right)\right], \end{aligned}$$

where Q is the quality factor of the lossy tank, and ω_0 is the resonant angular speed of the lossy tank. These are given by

$$Q = \frac{R}{\omega_0 L} = \frac{2\omega W_E}{P},$$

$$\omega_0^2 = \frac{1}{LC},$$

where P is the power dissipated in the resistor, and W_E is the time-averaged energy stored in the capacitor. The power P is related to the conductance G and the voltage V_t across the tank circuit by

$$|V_t|^2 G = P. \tag{5}$$

The circuit quantities are related to the antenna by choosing Q to be the antenna quality factor, and P to be the power radiated by the loaded-element resonant mode given by equation (3). The voltage V_t is

[3] See Appendix A for details of this computation.

[4] The series for W_E can also be accelerated, the details of which are given in Appendix A.

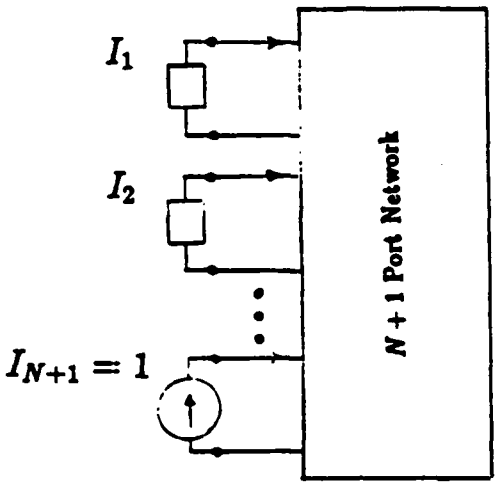

Figure 7: The $(N+1)$-port circuit model of a loaded element driven at port 1.

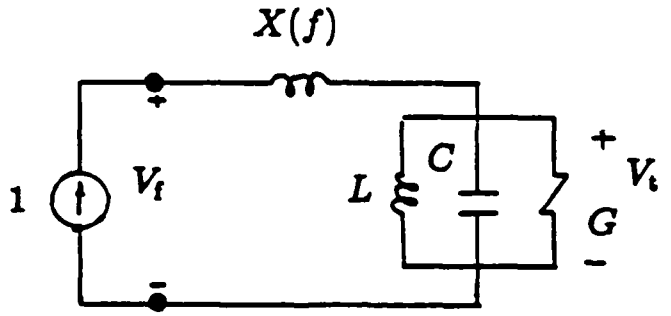

Figure 8: The circuit model for the input impedance of a loaded microstrip antenna.

$$V_t = -t\Psi(r_f),$$

where r_f is the center of the feed for the loaded element—the location of the $(N+1)^{st}$ port. Note that V_t is *not* the feed voltage V_f since the former *does not* include the effect of the feed reactance. The conductance G can thus be computed from equation (5).

The feed reactance, X_f, can be modeled as a linear process over the band of operation. Let the reactance corresponding to the lossless loaded cavity ($R = 0$) be denoted by X_r. Let the total reactance be $X(f)$. Let

$$X_f = X_{f0} + (f - f_0)X_{f1},$$

where f_0 corresponds to ω_0. Finally, let

$$f_+ = \left(1 + \frac{1}{2Q}\right) f_0,$$

$$f_- = \left(1 - \frac{1}{2Q}\right) f_0.$$

The resonant component of the reactance can be written as

$$X_r = \frac{2\pi L(f_0 + \Delta f)}{1 - (1 + \Delta f/f_0)^2},$$

where $\Delta f = f - f_0$. For small Δf, this can be written approximately as

$$X_r \approx -\pi L \frac{f_0^2}{\Delta f} - \pi L \frac{f_0}{2}.$$

Then,

$$X_{f0} \approx \frac{1}{2}(X(f_+) + X(f_-)) + \frac{\omega_0 L}{4}.$$

Similarly,

$$X_{f1} \approx \frac{Q}{f_0}\left[X(f_+) - X(f_-) + 2Q\omega_0 L\right].$$

The quantity $\omega_0 L = R/Q$ so that

$$X_{f0} \approx \frac{1}{2}(X(f_+) + X(f_-)) + \frac{R}{4Q},$$

and

$$X_{f1} \approx \frac{Q}{f_0}\left[X(f_+) - X(f_-) + 2R\right].$$

What remains is to determine the input reactance of the ideal cavity at the upper and lower frequencies f_+ and f_-.

Let the indices of the loaded ports be numbered from 1 to N with corresponding port voltages and currents of $V_1, , V_2, \ldots, V_N$ and $I_1, , I_2, \ldots, I_N$. The $(N+1)^{st}$ port is the feed port with feed current of $I_f = 1$ and feed voltage $V_f = Z_{in}$ where Z_{in} is the input impedance of the loaded element. If

$$\mathbf{V} = \begin{bmatrix} V_1 \\ V_2 \\ \vdots \\ V_N \end{bmatrix}$$

and I is redefined as

$$\mathbf{I} = \begin{bmatrix} I_1 \\ I_2 \\ \vdots \\ I_N \end{bmatrix}$$

then,

$$\begin{aligned} \mathbf{V} &= \mathbf{Z}\mathbf{I} + \mathbf{Z}_{mf} I_f, \\ V_f &= \mathbf{Z}_{mf}^t \mathbf{I} + Z_{ff}. \end{aligned}$$

The impedance matrix Z contains the multiport impedances between the *loaded* ports. The $(1 \times N)$-matrix $\mathbf{Z}_{mf}$ contains the mutual impedances between the feed port r_f and the load ports r_m. The self-impedance of the feed port in the unloaded cavity is Z_{ff}. Let the diagonal load impedance matrix be

$$\mathbf{Z}_L = \text{Diag}\left[Z_L^{(1)}, Z_L^{(2)}, \ldots, Z_L^{(N)}\right].$$

Then

$$\begin{aligned} \mathbf{V} &= -\mathbf{Z}_L \mathbf{I}, \\ \mathbf{I} &= -(\mathbf{Z} + \mathbf{Z}_L)^{-1} \mathbf{Z}_{mf}, \quad \text{and} \\ jX(f) &= V_f = Z_{ff} - \mathbf{Z}_{mf}^t (\mathbf{Z} + \mathbf{Z}_L)^{-1} \mathbf{Z}_{mf}. \end{aligned}$$

Having thus computed $X(f)$, one can now evaluate the input impedance Z_{in} of the antenna using

$$Z_{in} \approx X_{f0} + X_{f1}(f - f_0) + \frac{1}{G[1 + j2Q(f/f_0 - 1)]}.$$

As the results of the next section demonstrate, this expression is reasonably accurate over the band of a single resonant mode of the loaded element.

3 Application to Impedance Matching and Results

In this section, those elements of the theory presented in the previous sections specific to the application of varying impedance are presented together with corroborating experimental results. The objective in this application is to vary the input impedance *while keeping the resonant frequency and pattern of the element fixed.* This objective can be met by placing short-circuits at one or more appropriately chosen locations on the patch. These short-circuits can be PIN diodes thus allowing adaptation of the element to changing conditions such as the scan angle in a phased array. The theory and results given below assume that the loads are short circuits. One could probably also use voltage-controlled capacitors, varactor diodes. Use of varactors would probably simplify the biasing of the diodes. This possibility is currently under study.

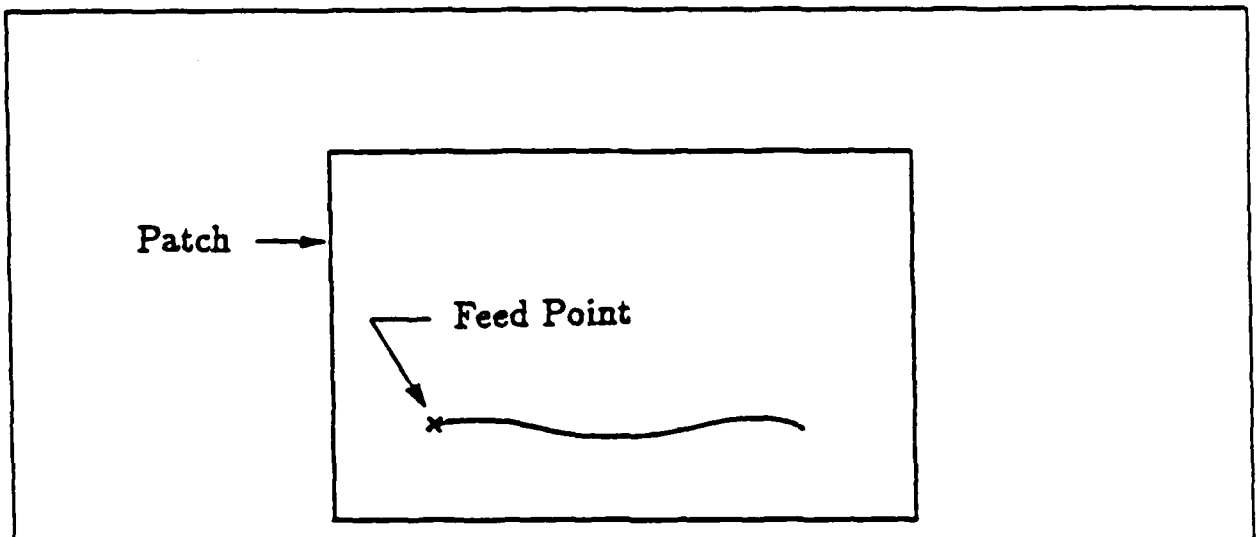

Figure 9: The locus of short-circuit locations for constant resonant frequency of the single-loaded element.

As seen in the previous section, one can vary the frequency by varying the location of a short circuiting pin. It is possible to vary the input impedance with a single short without altering the resonant frequency. The way that the input impedance is varied for a *fixed* feed location is to move the *nodal line* of the loaded resonant mode by moving the shorting pin location. The closer the nodal line is moved to the feed, the lower the peak input resistance will be. The trick is to move the shorting pin in such a way that at least the resonant frequency is unchanged. This was done using an interactive computer program with graphical output based on the theory discussed in the previous section.

3.1 Single short

The results of our computer program indicated that if a single short-circuit were placed on the locus illustrated in Fig. 9, then the resonant frequency of the resulting loaded elements should be identical. Using just a single short, one can vary the input impedance as is illustrated in Figs. 10–14. These figures contain the computed magnetic current distribution, the computed input impedance, and the measured input impedance of the loaded elements. In all cases, the patch dimensions were 4.00 cm wide by 6.00 cm long by 0.158 cm thick. The dielectric substrate was 3M Corporation's CuClad 250 glass reinforced, double clad PTFE. The manufacturer-supplied nominal dielectric constant was 2.43. The feed point was always at (1.00, 1.00), where the coordinates represent the distance in cm from a reference corner of the patch. The input impedance was collected using a computer-controlled, Hewlett-Packard 8410 network analyzer at the University of Houston.

It is quite clear from Figs. 10–14 that the magnetic current distributions around the edge of the patch are asymmetrical. The pattern that results from such a distribution will have a significant cross-polarized pattern

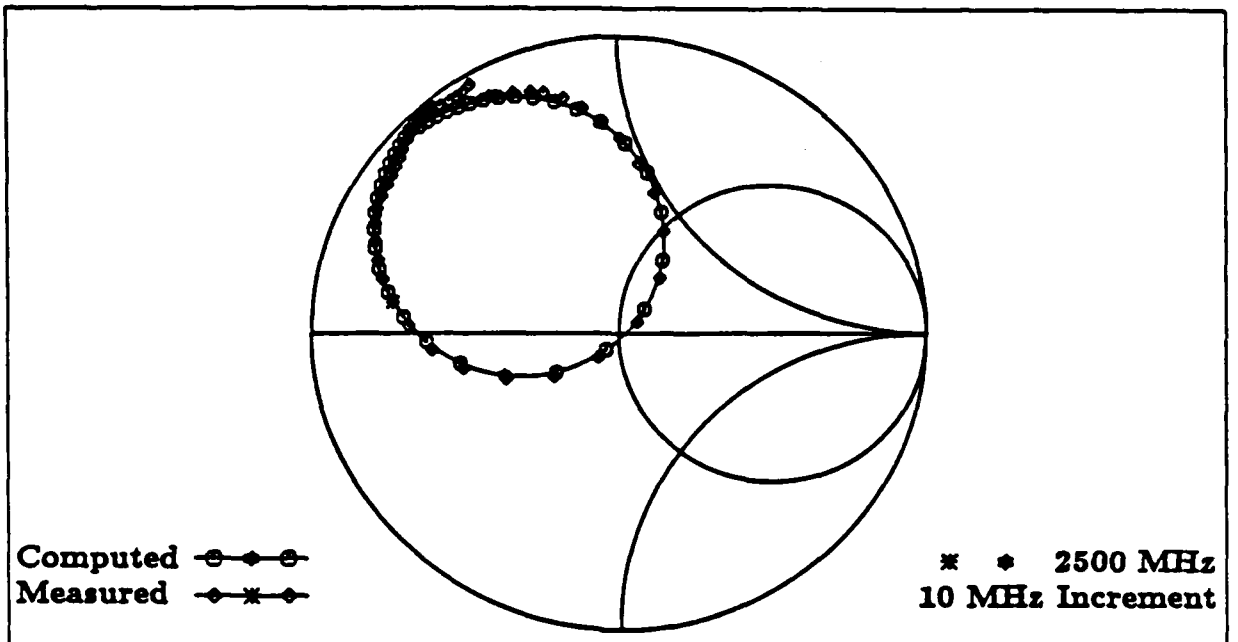

(a)

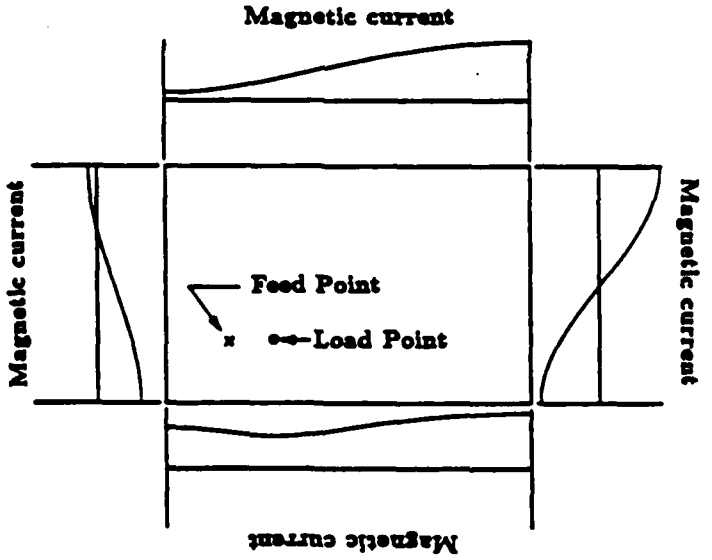

(b)

Figure 10: (a) Measured and computed input impedance of a single-loaded element with short-circuit at (1.75, 1.04). (b) Theoretical magnetic current distribution.

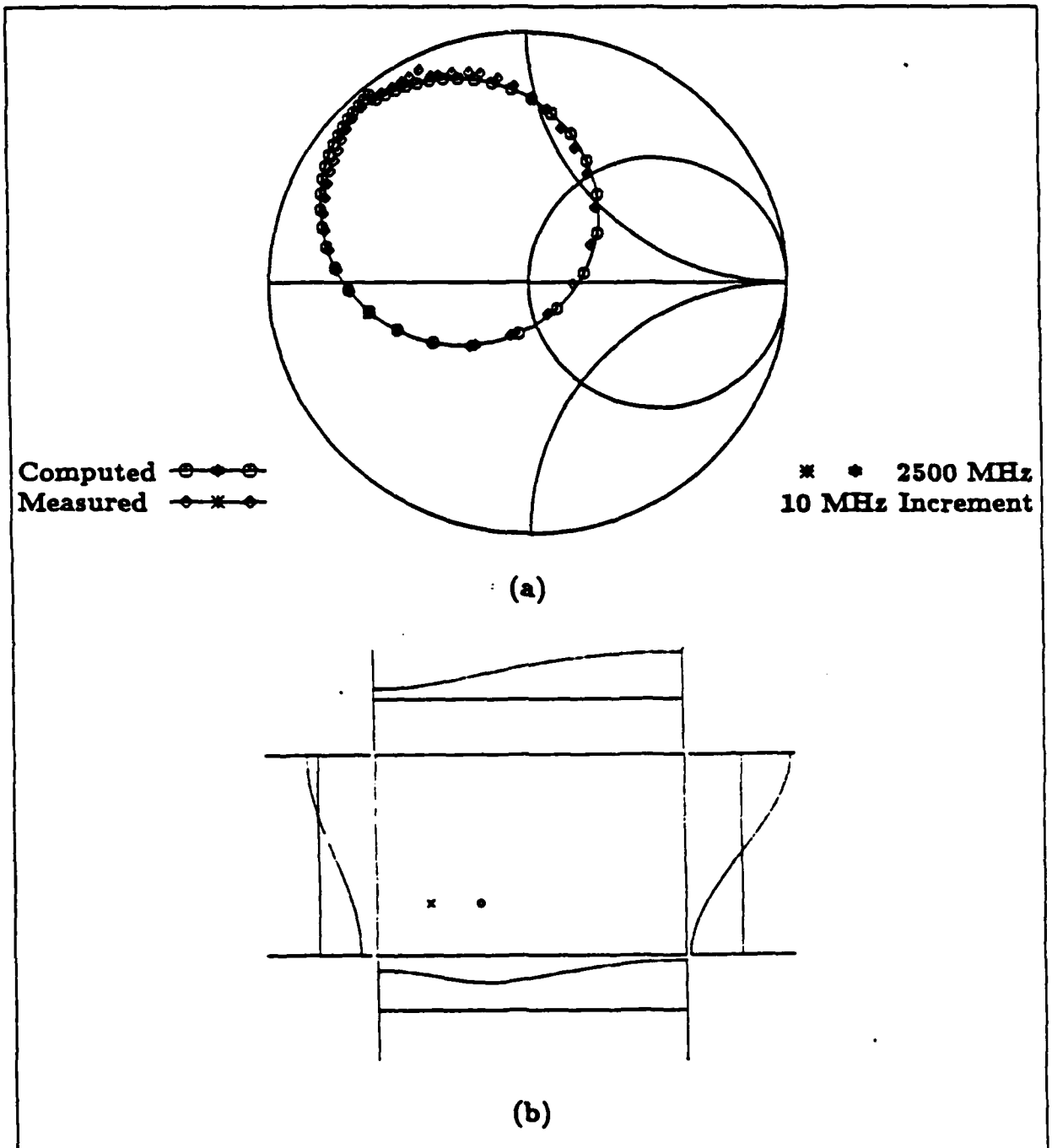

Figure 11: (a) Measured and computed input impedance of a single-loaded element with short-circuit at (2.00, 1.00). (b) Theoretical magnetic current distribution.

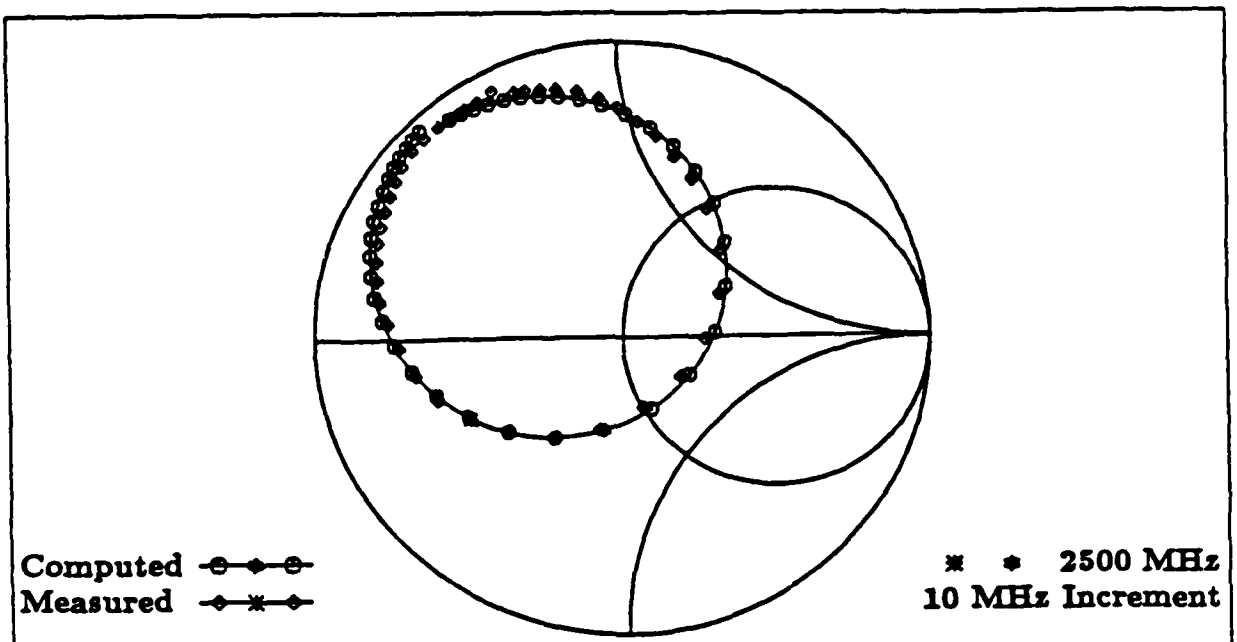

(a)

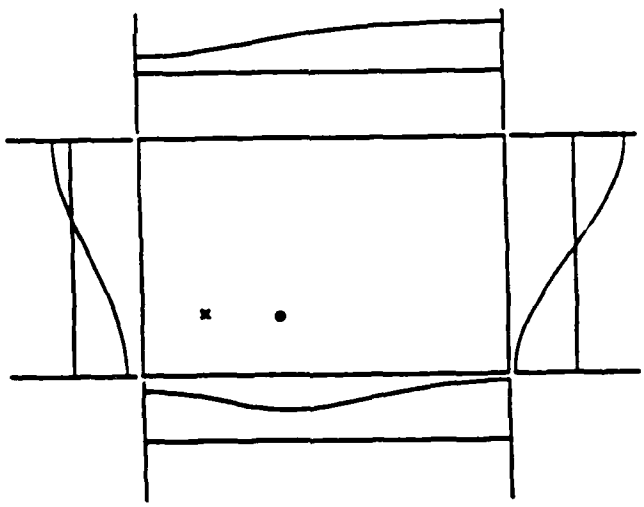

(b)

Figure 12: (a) Measured and computed input impedance of a single-loaded element with short-circuit at (2.25,0.95). (b) Theoretical magnetic current distribution.

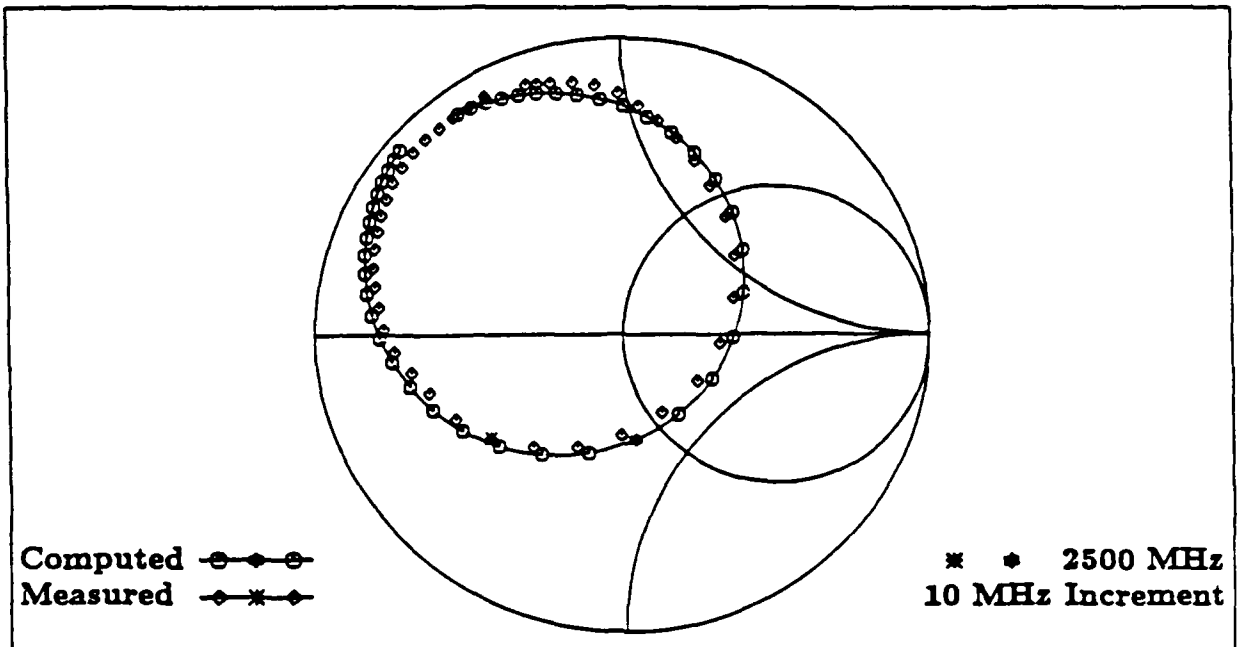

(a)

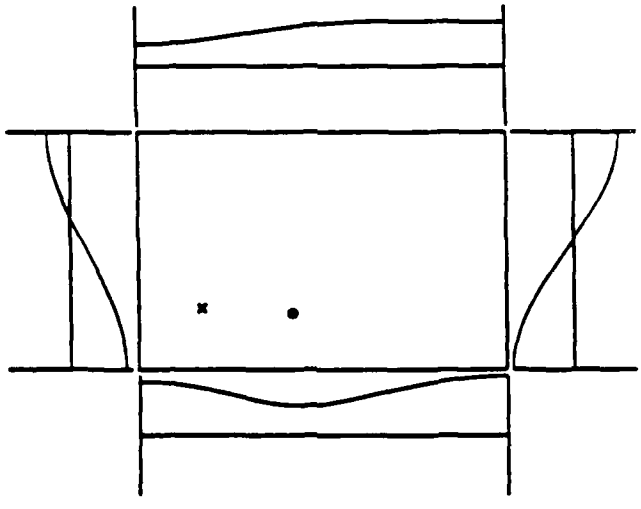

(b)

Figure 13: (a) Measured and computed input impedance of a single-loaded element with short-circuit at (2.50, 0.91). (b) Theoretical magnetic current distribution.

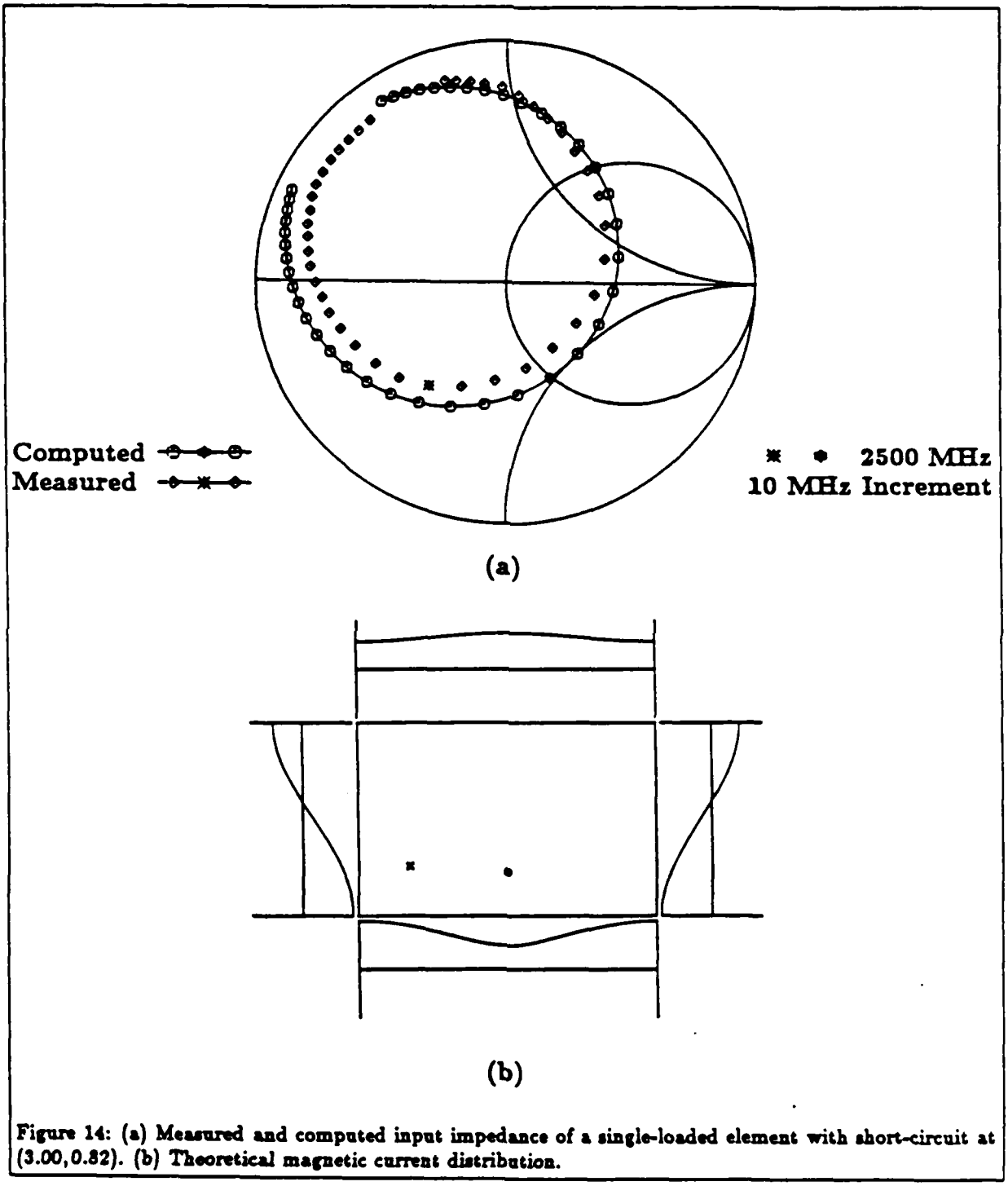

Figure 14: (a) Measured and computed input impedance of a single-loaded element with short-circuit at (3.00,0.82). (b) Theoretical magnetic current distribution.

although the E-plane pattern will be typical of the $(0,1)$-mode of a rectangular element. The theoretical and experimentally determined patterns for a patch loaded with a single short at $(2.50, 0.91)$ are illustrated in Fig. 15. The measured patterns were taken with the element mounted on a 1.05m (8.7-wavelength) circular ground plane. The element was driven at a frequency of 2470 MHz. Our pattern range is fairly new; it is difficult to say how much of the cross-polarization is due to errors introduced by the range and how much is due to the asymmetry in the element's magnetic current distribution. Nevertheless, the cross-polarized patterns appear to be at least qualitatively consistent with the predicted patterns. Note that some of the discrepancy, especially the scalloping of the pattern and the loss of gain at the horizon is due to the finite size of the ground plane.

In any case, it is clear that the cross-polarization arising when a single short circuit is used is significant and probably unacceptable in many applications. Because of this, at least two shorts should be used in symmetrical locations. There is another reason why two or more shorts should be used. It is clear from the measured and computed input impedances that the impedance range obtained is not extremely broad for a single-loaded element. We did not measure impedance levels for shorts any closer to the feed than those illustrated in Figs. 10–14 because of the obstruction caused by mounting an SMA feed. However we have plotted the theoretical resistance R *versus* x, where x is the x-coordinate of a single short-circuit placed along the locus illustrated in Fig. 9. This plot is contained in Fig. 16. This result should be compared with the results for the double-loaded elements considered next.

3.2 Two shorts

With *two* shorts located symmetrically with respect to the long center line of the patch one can eliminate the cross-polarization in the H-plane. Furthermore, one can more easily obtain a wider variation of input impedance. Figures 17–19 contain the theoretical magnetic current distribution, and the measured and computed input impedances of elements loaded by symmetrically located pairs of short-circuits. The locus of points on which these pairs of short-circuits should lie is illustrated in Fig. 20.

The theoretical and measured patterns are given in Fig. 21. The measured cross-polarization is disappointingly high in this case. As mentioned before, this may be due to errors introduced by the range. Nevertheless, the cross-polarization is definitely reduced from what it was in the case of the single-loaded element.

Finally, it is clear from Figs. 17–19 and Fig. 22 that the impedance variation is greater for the double-loaded element than for the single-loaded element. In short, it appears that the performance yielded by a single short falls short of that obtainable using two shorts.

4 Conclusions and Future Research

There are several conclusions that can be drawn from the theory and results presented in this report.

1. It is possible to change the input impedance of a microstrip element over a wide range without affecting its resonant frequency or co-polar pattern by moving short-circuits from one point to another.

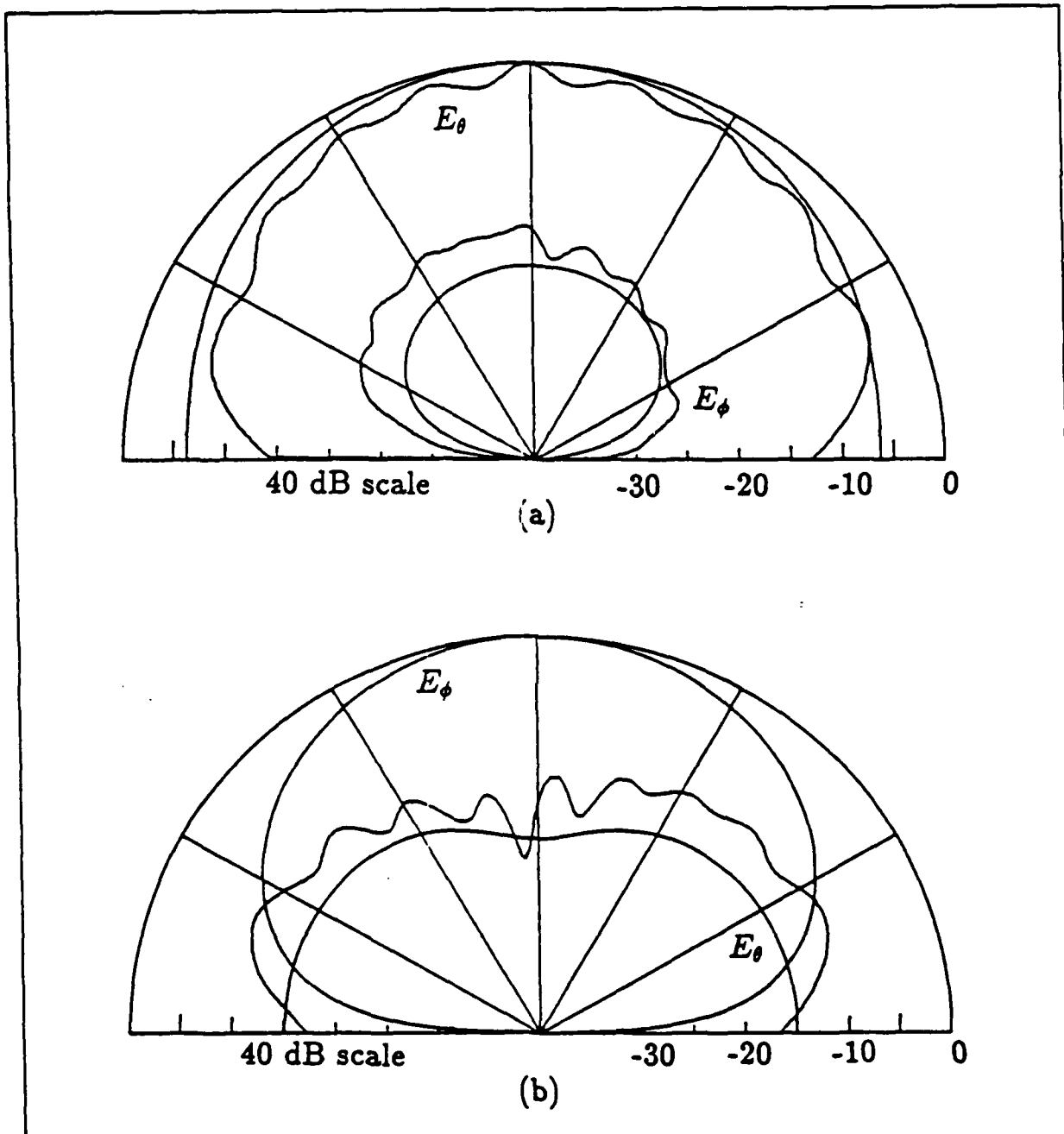

Figure 15: (a) Measured and computed input co-polar and cross-polar patterns in the *E*-plane for a short-circuit at (2.50,0.91). (b) Measured and theoretical patterns in *H*-plane.

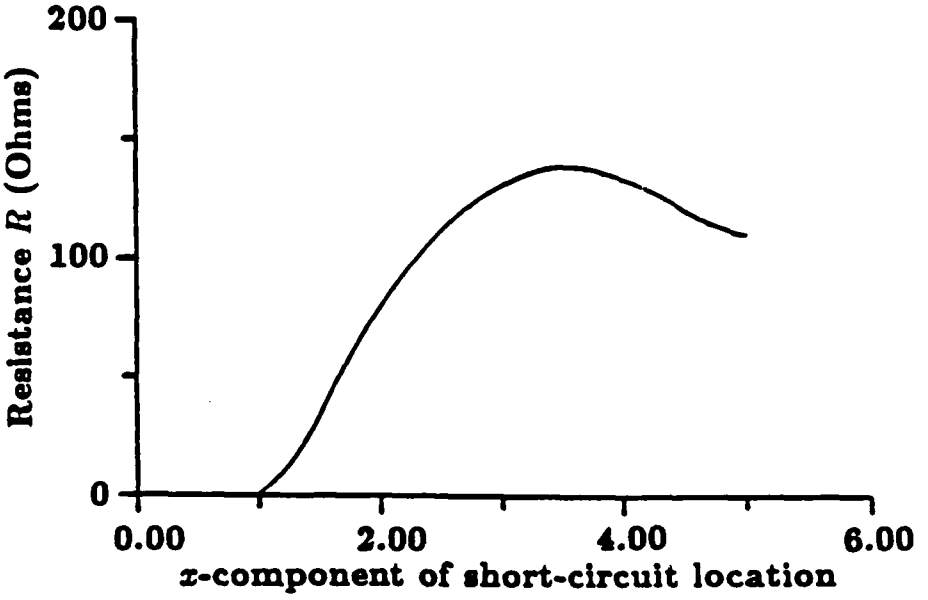

Figure 16: The variation of the conductance G with the x-coordinate of a short position taken from the constant resonant frequency locus for a fixed feed at (1.00, 1.00).

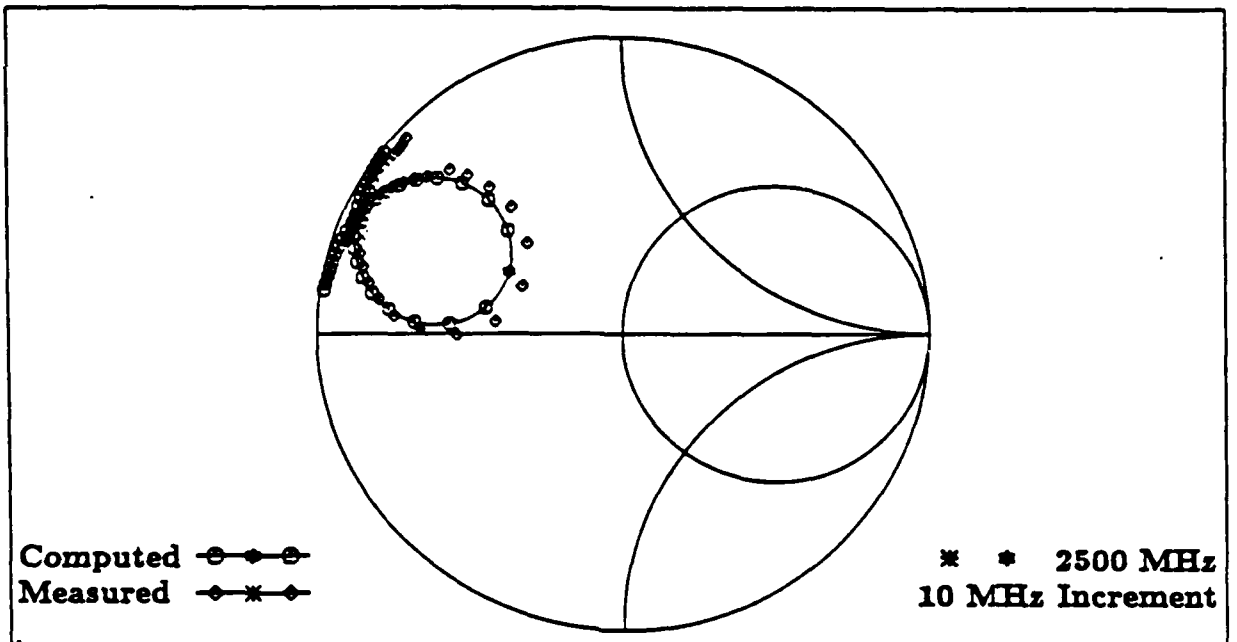

(a)

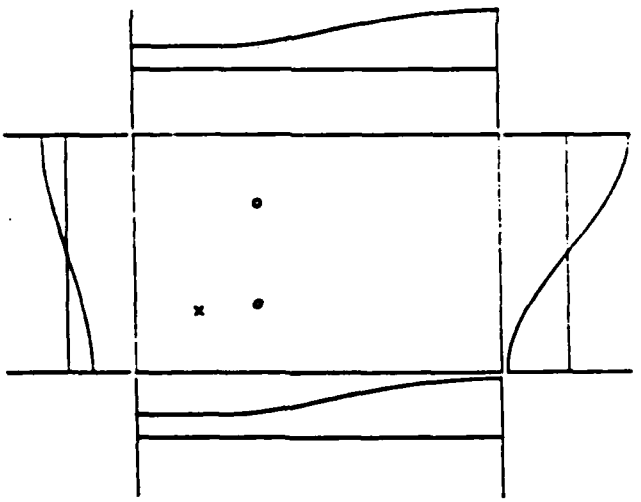

(b)

Figure 17: (a) Measured and computed input impedance of a double-loaded element with short-circuits at (2.00, 1.12) and (2.00, 2.88). (b) Theoretical magnetic current distribution.

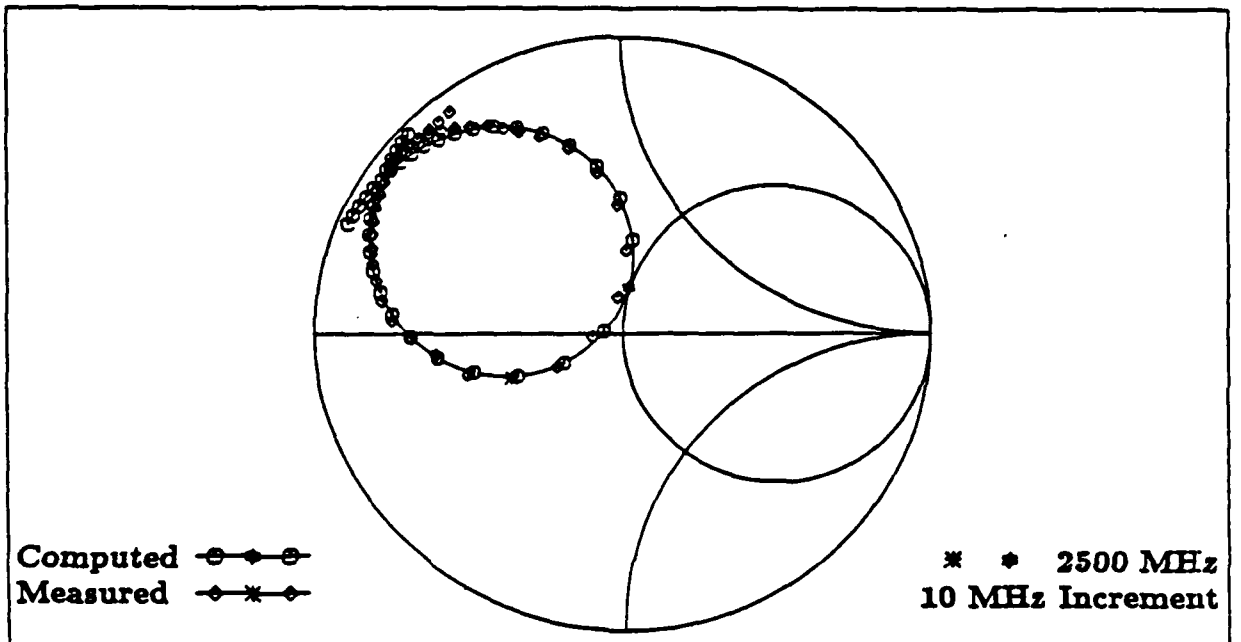

(a)

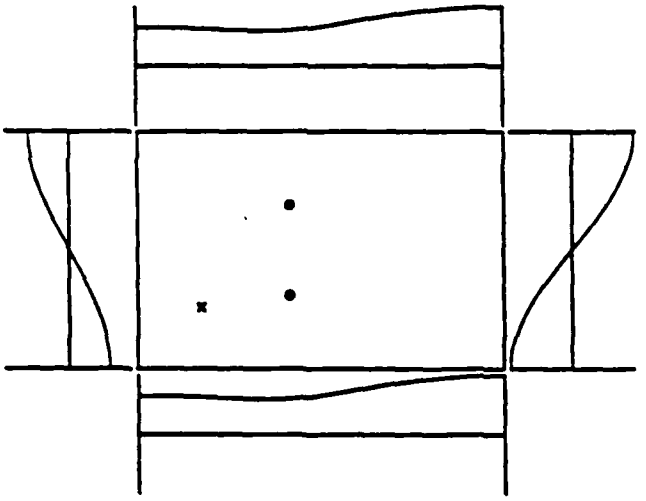

(b)

Figure 18: (a) Measured and computed input impedance of a double-loaded element with short-circuits at (2.50, 1.21) and (2.50, 2.79). (b) Theoretical magnetic current distribution.

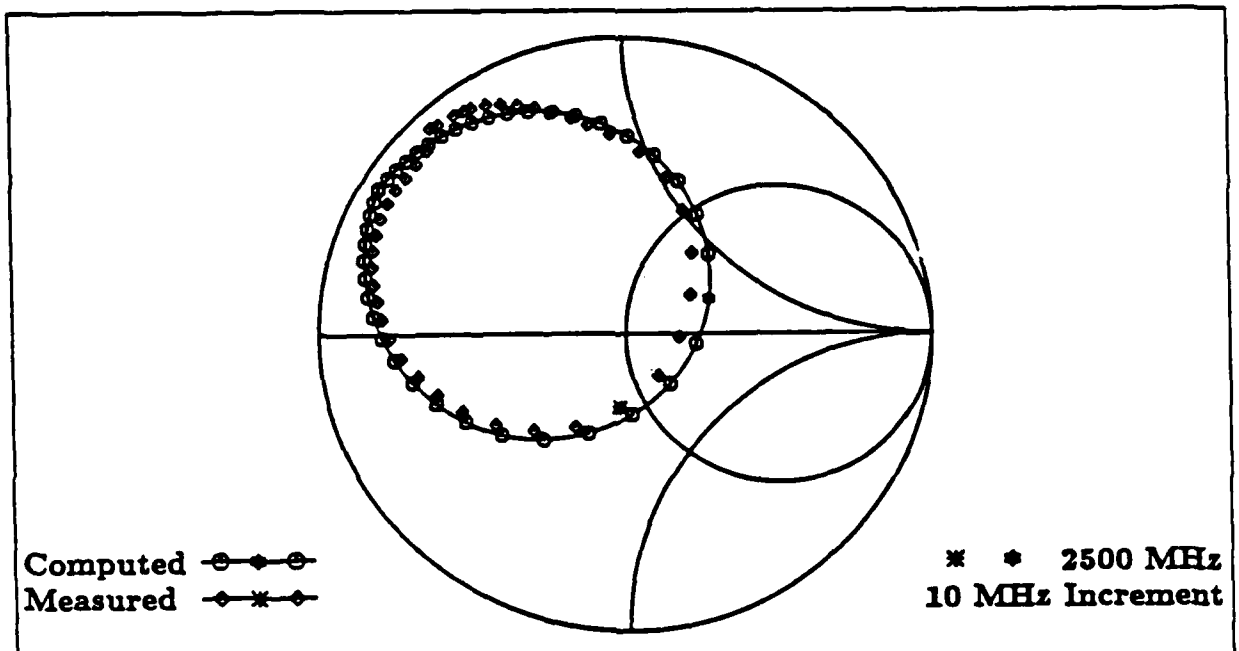

(a)

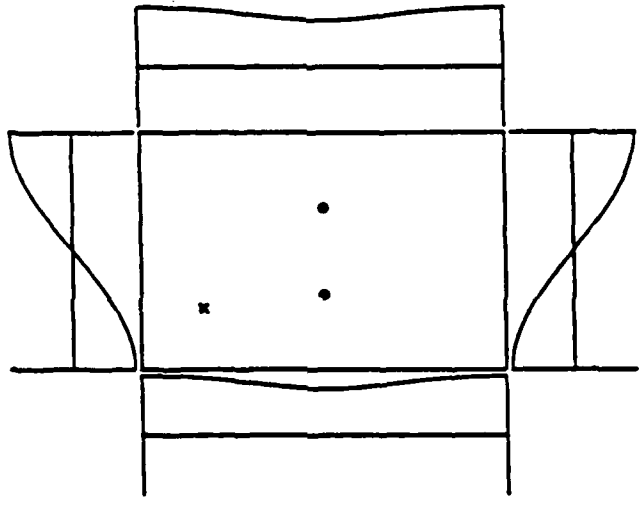

(b)

Figure 19: (a) Measured and computed input impedance of a double-loaded element with short-circuits at (3.00, 1.23) and (3.00, 2.77). (b) Theoretical magnetic current distribution.

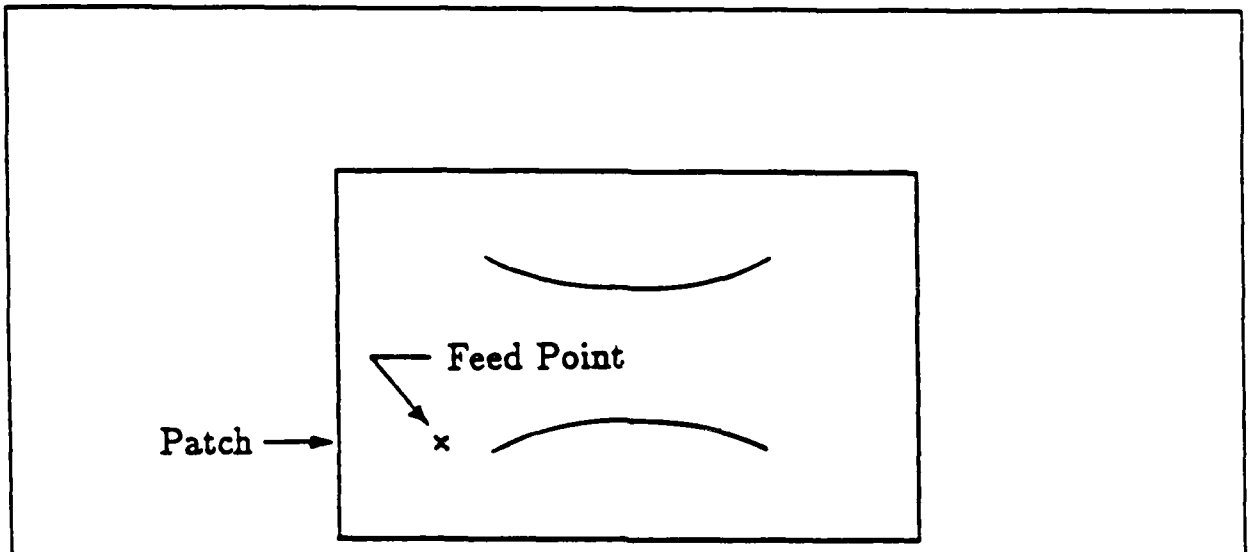

Figure 20: The locus of short-circuit locations for constant resonant frequency of the double-loaded element.

2. The theory that predicts this result has been corroborated by experiment. Specifically, the experiment shows that the resonant frequency of the mode is left relatively unchanged by the appropriate placement of short-circuits. Small deviations between the predicted and observed resonant frequency do exist. They are due partly to errors in fabrication of the element and partly due to the errors introduced by the cavity model upon which the theory is based. The experiment also shows that the agreement between the predicted and observed input impedance is excellent in most cases. Finally, there was qualitative agreement between theoretical patterns and measured patterns although the measured cross-polarized components in the double-loaded element were much higher than expected from the theory—possibly a problem with our range and ground plane fixture.

3. From the point of view of producing lower cross-polarization and from the point of view of more easily varying the impedance level over a wide range, two short-circuits are better than one short-circuit. Each short-circuit pair should be biased together with the same biasing voltage.

Some important items are left for future research. These include the following.

1. A simulation of loaded elements in a phased array needs to be carried out to determine the basic feasibility of the ultimate application. This, we propose, as the major deliverable of a future research contract.

2. Because each diode or diode pair needs a biasing line, the number of biasing lines could become quite large if many levels of adjustment in impedance are provided. For this reason, we are currently studying the feasibility of using voltage-controlled capacitors to change the impedance level.

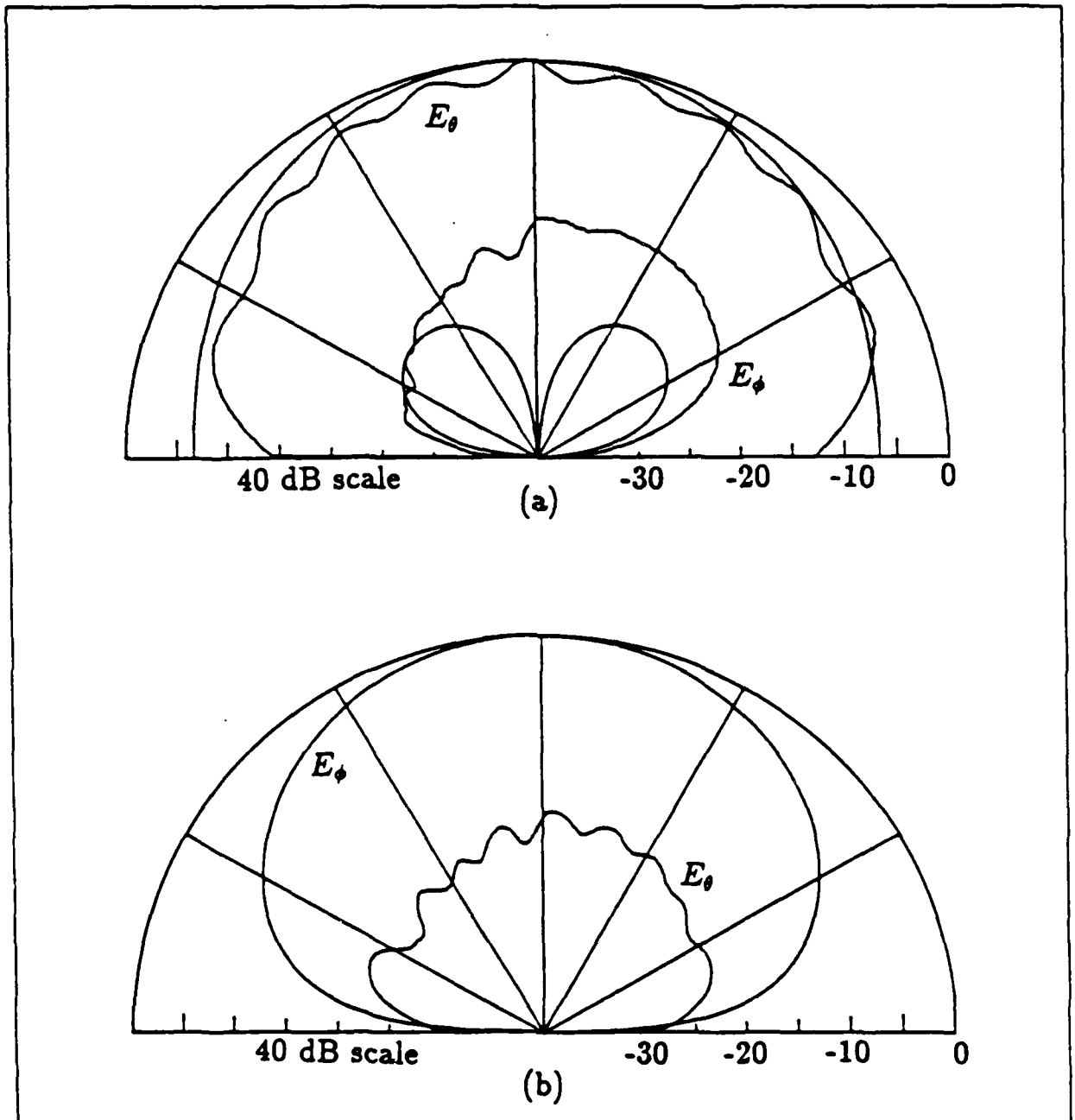

Figure 21: (a) Measured and computed input co-polar and cross-polar patterns in the E-plane for short-circuits at (2.00, 1.12) and (2.00, 2.88). (b) Measured and theoretical patterns in H-plane.

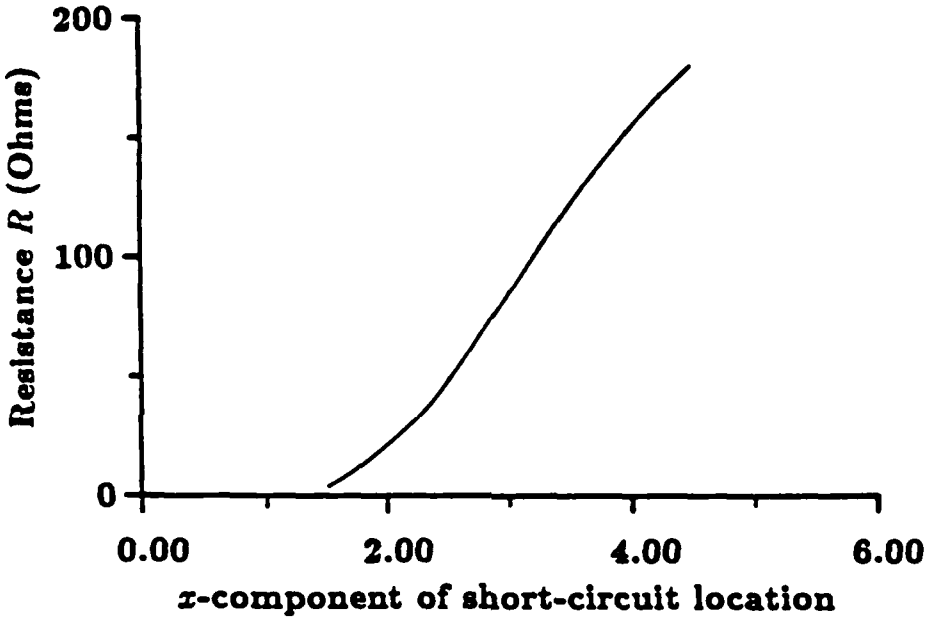

Figure 22: The variation of the conductance G with the x-coordinate of a short position taken from the constant resonant frequency locus for a fixed feed at (1.00, 1.00).

A Additional Theoretical Results

This appendix contains additional theoretical results that are implemented in the computer program used to generate the data presented in Section 3. There are three topics within this appendix:

1. The efficient computation of the cavity Green's function,
2. The computation of the far-field pattern, and
3. The computation of the energy stored in the cavity.

A.1 The efficient computation of the cavity Green's function

The expression for the Green's function in equation (1) is very slowly converging and not particularly useful, especially for patches of other than rectangular shape. It can be accelerated in the following way. First partition the set A of mode indices into the union of three sets,

$$A = \{(0,0)\} \cup \overline{A}_\xi \cup A_\xi.$$

The first set, consisting of a single element, represents the indices of the "D.C. mode." This is the mode of the unloaded cavity that resonates at zero frequency—it is just a constant. Since the modes are assumed to be normalized, this constant is

$$\psi_{00}(\boldsymbol{r}) = \frac{1}{\sqrt{S}},$$

where S represents the area of the patch.[5] The third set is the set of modes whose resonant wavenumbers are greater than or equal to $\xi k_{\max}$:

$$A_\xi = \{(m,n) | k_{mn} \geq \xi k_{\max}\}.$$

The parameter $k_{\max}$ is the

$$k_{\max} = \frac{2\pi f_{\max}\sqrt{\epsilon_r \mu_r}}{c},$$

where c is the speed of light in a vacuum, and $f_{\max}$ is the maximum frequency of interest for the antenna—a number that can be specified *a priori* for any analysis. The parameter ξ is some real constant greater than one. The second set is the complement of A_ξ with respect to the set A_0,

$$\overline{A}_\xi = A_0 - A_\xi,$$

where

$$A_0 = A - \{(0,0)\}$$

is the set of all mode index pairs *except* for that corresponding to the D.C. mode.

Suppose that $|\zeta| \leq 1/\xi$. Then one can approximate the fraction $1/(1-\zeta^2)$ by

[5] The same symbol is used to represent the set of points making up the patch. No confusion between the two uses should arise.

$$\frac{1}{1-\zeta^2} \approx a_0 + a_1\zeta^2 + a_2\zeta^4 + \cdots + a_{L-1}\zeta^{2(L-1)}.$$

Then for mode indices in A_ξ, one can approximate the fraction $1/(k^2 - k_{mn}^2)$ by

$$\frac{1}{k^2 - k_{mn}^2} \approx -a_0\frac{1}{k_{mn}^2} - a_1\frac{k^2}{k_{mn}^4} - \cdots - a_{L-1}\frac{k^{2L-2}}{k_{mn}^{2L}}.$$

Thus, the sum in equation (1) can be partitioned and approximated as

$$G(\mathbf{r}|\mathbf{r}') \approx j\omega\mu\left\{\frac{1}{S} + \sum_{\overline{A}_\xi}\frac{\psi_{mn}(\mathbf{r})\psi_{mn}(\mathbf{r}')}{k^2 - k_{mn}^2} - a_0\sum_{A_\xi}\frac{\psi_{mn}(\mathbf{r})\psi_{mn}(\mathbf{r}')}{k_{mn}^2}\right.$$
$$\left. - a_1k^2\sum_{A_\xi}\frac{\psi_{mn}(\mathbf{r})\psi_{mn}(\mathbf{r}')}{k_{mn}^4} - \cdots - a_{L-1}k^{2L-2}\sum_{A_\xi}\frac{\psi_{mn}(\mathbf{r})\psi_{mn}(\mathbf{r}')}{k_{mn}^{2L}}\right\}.$$

This sum can be recast in a more convenient form for acceleration by summing over A_0 instead of A_ξ The result is

$$G(\mathbf{r}|\mathbf{r}') \approx j\omega\mu\left\{\frac{1}{S} + \sum_{\overline{A}_\xi}\left[\frac{1}{k^2 - k_{mn}^2} + a_0\frac{1}{k_{mn}^2} + a_1\frac{k^2}{k_{mn}^4} + \cdots + a_{L-1}\frac{k^{2L-2}}{k_{mn}^{2L}}\right]\psi_{mn}(\mathbf{r})\psi_{mn}(\mathbf{r}')\right.$$
$$- a_0\sum_{A_0}\frac{\psi_{mn}(\mathbf{r})\psi_{mn}(\mathbf{r}')}{k_{mn}^2} - a_1k^2\sum_{A_0}\frac{\psi_{mn}(\mathbf{r})\psi_{mn}(\mathbf{r}')}{k_{mn}^4}$$
$$\left. - \cdots - a_{L-1}k^{2L-2}\sum_{A_0}\frac{\psi_{mn}(\mathbf{r})\psi_{mn}(\mathbf{r}')}{k_{mn}^{2L}}\right\}.$$

There are compromises to be made in the choice of the parameter ξ. If ξ is chosen too near 1, then the required number of terms L necessary to approximate the fraction $1/(1-\zeta^2)$ becomes very large. On the other hand, if ξ is chosen to be much greater than 1, L may be small, but the number of elements in the set $\overline{A}_\xi$ becomes very large. Either of these conditions is undesirable. A reasonable choice of ξ is $\xi = 2$. If L is then chosen to be 2, and the coefficients a_0 and a_1 are chosen to be 0.989 and 1.331, respectively, the error in the approximation is about one percent. Thus, the Green's function can be approximated as

$$G(\mathbf{r}|\mathbf{r}') = j\omega\mu\left\{\frac{1}{S} + \sum_{\overline{A}_\xi}\left[\frac{1}{k^2 - k_{mn}^2} + a_0\frac{1}{k_{mn}^2} + a_1\frac{k^2}{k_{mn}^4}\right]\psi_{mn}(\mathbf{r})\psi_{mn}(\mathbf{r}')\right. \tag{6}$$
$$\left. + a_0G_0(\mathbf{r}|\mathbf{r}') + k^2a_1G_1(\mathbf{r}|\mathbf{r}')\right\},$$

where

$$G_0(\mathbf{r}|\mathbf{r}') = -\sum_{A_0}\frac{\psi_{mn}(\mathbf{r})\psi_{mn}(\mathbf{r}')}{k_{mn}^2},$$

$$G_1(\mathbf{r}|\mathbf{r}') = -\sum_{A_0} \frac{\psi_{mn}(\mathbf{r})\psi_{mn}(\mathbf{r}')}{k_{mn}^4}.$$

The decomposition of the Green's function expressed in equation (6) represents an expansion of G in terms of its first few lowest-order modes plus the contribution due to all higher-order modes, a quasistatic expansion. Once the quasistatic terms $G_0(\mathbf{r}|\mathbf{r}')$ and $G_1(\mathbf{r}|\mathbf{r}')$ are computed, then the Green's function can be evaluated very efficiently for different frequencies—the most difficult part will have been done once and for all for a given pair of source and observation points $\mathbf{r}$ and $\mathbf{r}'$.

The series for $G_0(\mathbf{r}|\mathbf{r}')$ and $G_1(\mathbf{r}|\mathbf{r}')$ are still very slowly converging, as slowly converging as the series for G. These quasistatic Green's functions satisfy the boundary-value problem,

$$\nabla^2 G_0(\mathbf{r}|\mathbf{r}') = \delta(\mathbf{r}-\mathbf{r}') - \frac{1}{S}, \quad \mathbf{r} \in S,$$

$$\nabla G_0(\mathbf{r}|\mathbf{r}')\cdot\hat{\mathbf{n}} = 0, \quad \mathbf{r} \in \partial S;$$

$$\nabla^2 G_1(\mathbf{r}|\mathbf{r}') = -G_0(\mathbf{r}|\mathbf{r}'), \quad \mathbf{r} \in S,$$

$$\nabla G_1(\mathbf{r}|\mathbf{r}')\cdot\hat{\mathbf{n}} = 0, \quad \mathbf{r} \in \partial S.$$

One can obtain G_0 and G_1 by evaluating

$$G_0 = \frac{1}{j\omega\mu} \lim_{k\to 0} \left(G - \frac{j\omega\mu}{k^2 S} \right), \tag{7}$$

$$G_1 = \frac{1}{j\omega\mu} \lim_{k\to 0} \left\{ \frac{\partial}{\partial k^2} \left(G - \frac{j\omega\mu}{k^2 S} \right) \right\}. \tag{8}$$

By expanding G in a Laurant series in k^2 about $k^2 = 0$, one can evaluate these limits. To this end, the patch is first described in terms of a coordinated system appropriate to the patch shape.

Let u and v be the coordinate variables of an orthogonal coordinate system derived through a conformal mapping of the rectangular coordinate system. This mapping is chosen so that it maps the patch into a rectangular patch in the (u,v)-plane. Of course, if the patch is already rectangular, then $u = x$, $v = y$. For a circular patch, a circular sector patch, an annular patch, or an annular sector patch, the transformation used is

$$x = ae^v \cos u,$$

$$y = ae^v \sin u,$$

where a is the outer radius of the patch. The transformation need not be analytic, but it must satisfy

$$\left|\frac{\partial u}{\partial x}\right| = \left|\frac{\partial v}{\partial y}\right|,$$

$$\left|\frac{\partial v}{\partial x}\right| = \left|\frac{\partial u}{\partial y}\right|.$$

If these equations are satisfied, then the boundary value problem for G is transformed into

$$[\nabla^2 + k^2 h(u,v)^2] G(\mathbf{r}|\mathbf{r}') = j\omega\mu\delta(\mathbf{r} - \mathbf{r}'),$$

where $h(u,v)$ is the common scale factor of the u and v variables. If the patch is separable, then

$$h(u,v)^2 = f(u) + g(v).$$

In this case, G can be expressed as

$$G(\mathbf{r}|\mathbf{r}') = j\omega\mu \sum_{m=0}^{\infty} \frac{U_m(u)U_m(u')V_m^-(v_<)V_m^+(v_>)}{N_m W\left(V_m^-, V_m^+\right)}, \tag{9}$$

where

$$N_m = \int_{u_-}^{u_+} U_m(u)^2 du,$$

$$W\left(V_m^-, V_m^+\right) = W_m = V_m^-(v_+)V_m^{+\prime}(v_+) - V_m^{-\prime}(v_+)V_m^+(v_+),$$

$$v_< = \begin{cases} v, & v < v' \\ v', & v' < v \end{cases},$$

$$v_> = \begin{cases} v, & v' < v \\ v', & v < v' \end{cases}.$$

The prime "$\prime$" on *dependent* variables indicates differentiation with respect to argument. The primes on u and v indicate the source point location (u', v') in the (u,v)-coordinate system. The U_m's and V_m's satisfy the separated Helmholtz equations,

$$U_m'' + \left(\alpha_m^2 + k^2 f(u)\right) U_m = 0,$$

$$V_m'' + \left(-\alpha_m^2 + k^2 g(v)\right) V_m = 0,$$

where the "$\pm$" superscript has been suppressed on the "V" for convenience.

The α_m^2 is the separation constant determined by applying the pair of homogeneous boundary conditions that $U_m(u)$ satisfies at $u = u_\pm$, where u_- is the left boundary of the transformed patch and u_+ is its right boundary. Similarly, v_- is the lower boundary of the transformed patch and v_+ is its upper boundary. These boundary conditions depend on the geometry of the patch. They are either the physical boundary condition that the derivative $U_m(u)$ must vanish at one or both of the limits of u, or that $U_m(u)$ must satisfy conditions that will make the field and its derivatives continuous at the limits of u. Without loss of generality, one can always assume that $V_m^{+\prime}(v_+) = 0$. The condition that $V_m^-(v)$ satisfies can also be the physical boundary condition that its derivative vanishes at $v = v_-$, or that the field be continuous at $v = v_-$.

These parameters can be expanded in a power series in k^2 as

$$U_m = U_{0m} + k^2 U_{1m} + k^4 U_{2m} + \cdots,$$

$$V_m = V_{0m} + k^2 V_{1m} + k^4 V_{2m} + \cdots,$$

$$\alpha_m^2 = \alpha_{0m}^2 + k^2 \alpha_{1m}^2 + k^4 \alpha_{2m}^2 + \cdots,$$

$$N_m = N_{0m} + k^2 N_{1m} + k^4 N_{2m} + \cdots,$$

$$W_m = W_{0m} + k^2 W_{1m} + k^4 W_{2m} + \cdots.$$

The U_{nm}'s and the $V_{nm}^{\pm}$'s satisfy the sequence of differential equations,

$$U_{nm}'' + \alpha_{0m}^2 U_{nm} = -\sum_{\ell=0}^{n-1} \alpha_{(n-\ell),m}^2 U_{\ell m} - f(u) U_{(n-1),m},$$

$$V_{nm}'' - \alpha_{0m}^2 V_{nm} = \sum_{\ell=0}^{n-1} \alpha_{(n-\ell),m}^2 V_{\ell m} - g(v) V_{(n-1),m},$$

where again the superscript "$\pm$" on the V's has been dropped for convenience. In addition to applying the boundary conditions discussed above, the following conditions are also applied to obtain the solution in the most convenient form:

$$N_{1m} = N_{2m} = \cdots = 0,$$

$$V_{nm}^{+}(v_+) = 0, \quad n > 0,$$

$$V_{0m}^{+}(v_+) = 1,$$

$$V_{nm}^{-}(v_-) = 0, \quad n > 0,$$

$$V_{0m}^{-}(v_-) = 1.$$

These conditions can be applied since any of the multiplication of the U and V functions by any arbitrary function of k^2 leaves $G(r|r')$ unchanged, but *does change* the coefficients of the series in k^2 listed above—i.e., the expansions given above are *not* unique. This choice simplifies the coefficients of the expansion of the Wronskian; they become

$$W_{nm} = -V_{nm}^{-\prime}(v_+).$$

Using the solutions of these equations in equations (7), (8), and (9) yields the expressions

$$G_\ell(r|r') = r_{\ell 0} + \sum_{m=0}^{\infty} r_{\ell m}.$$

The r's are

$$r_{00} = \frac{1}{S}\left\{ n_{10} - \frac{\Delta u}{S} W_{20} \right\},$$

$$r_{10} = \frac{1}{S}\left\{ n_{20} - n_{10}\frac{\Delta u}{S} W_{20} - \frac{\Delta u}{S} W_{30} + \left(\frac{\Delta u}{S} W_{20}\right)^2 \right\},$$

$$r_{0m} = \frac{2n_{0m}}{\Delta u W_{0m}}, \qquad m > 0,$$

$$r_{1m} = \left\{ n_{1m} - \frac{n_{0m} W_{1m}}{W_{0m}} \right\} \frac{2}{\Delta u W_{0m}}, \qquad m > 0,$$

where $\Delta u = u_+ - u_-$. The n's are given by

$$\begin{aligned}
n_{0m} &= U_{0m}(u) U_{0m}(u') V_{0m}^-(v_<) V_{0m}^+(v_>), \\
n_{1m} &= U_{1m}(u) U_{0m}(u') V_{0m}^-(v_<) V_{0m}^+(v_>) + U_{0m}(u) U_{1m}(u') V_{0m}^-(v_<) V_{0m}^+(v_>) \\
&\quad + U_{0m}(u) U_{0m}(u') V_{1m}^-(v_<) V_{0m}^+(v_>) + U_{0m}(u) U_{0m}(u') V_{0m}^-(v_<) V_{1m}^+(v_>), \\
n_{20} &= U_{20}(u) + U_{20}(u') + V_{20}^-(v_<) + V_{20}^+(v_>) \\
&\quad + U_{10}(u) U_{10}(u') + V_{10}^-(v_<) V_{10}^+(v_>) \\
&\quad + U_{10}(u) V_{10}^-(v_<) + U_{10}(u) V_{10}^+(v_>) + U_{10}(u') V_{10}^-(v_<) + U_{10}(u') V_{10}^+(v_>).
\end{aligned}$$

The summand of G_0 always contains the term

$$\frac{j\omega\mu}{2\pi} \Re \left\{ \frac{1}{m} e^{-m\nu z} \right\},$$

where $\alpha_{0m} = m\nu$, $z = v_> - v_< + j(u - u')$. This term can be summed in closed form to yield

$$G_0(r|r') = \frac{j\omega\mu}{2\pi} \left\{ \nu \frac{v_> - v_<}{2} - \ln|\nu z| - \ln \left| \frac{\sinh(\nu z/2)}{\nu z/2} \right| \right\} + \text{remainder terms.}$$

For source points (u', v') not on the edge of the patch, the remainder terms of G_0 in the preceeding expression are non-singular as $(u, v) \to (u', v')$ The logarithmic singularity of the Green's function is explicitly extracted by this method. The remainder terms of G_0 and of G_1 involve sums over m of terms of the form

$$\frac{e^{-m\nu z_i}}{(m\nu)^\ell}$$

where z_i is a complex number whose real and imaginary parts are linear functions of u, u', v, and v', and $\ell = 1, 2, 3, \ldots$

The series associated with these terms can be evaluated efficiently using the functions

$$F_n(z) = \Re \left\{ \sum_{\ell=1}^{\infty} \frac{e^{-\ell z}}{\ell^n} \right\}, \quad \ell = 1, 2, \ldots, \quad \Re\{z\} \geq 0.$$

The first function $F_1(z)$ can be summed in terms of elementary functions and is given by

$$F_1(z) = \frac{\Re\{z\}}{2} - \ln\{2|\sinh(z/2)|\}.$$

The second and third functions $F_2(z)$ and $F_3(z)$ can be computed for z in various regions of the complex z-plane as indicated in Figs. 23-24.The formulas are extended by the following identities to regions of the complex z-plane not covered in these two figures:

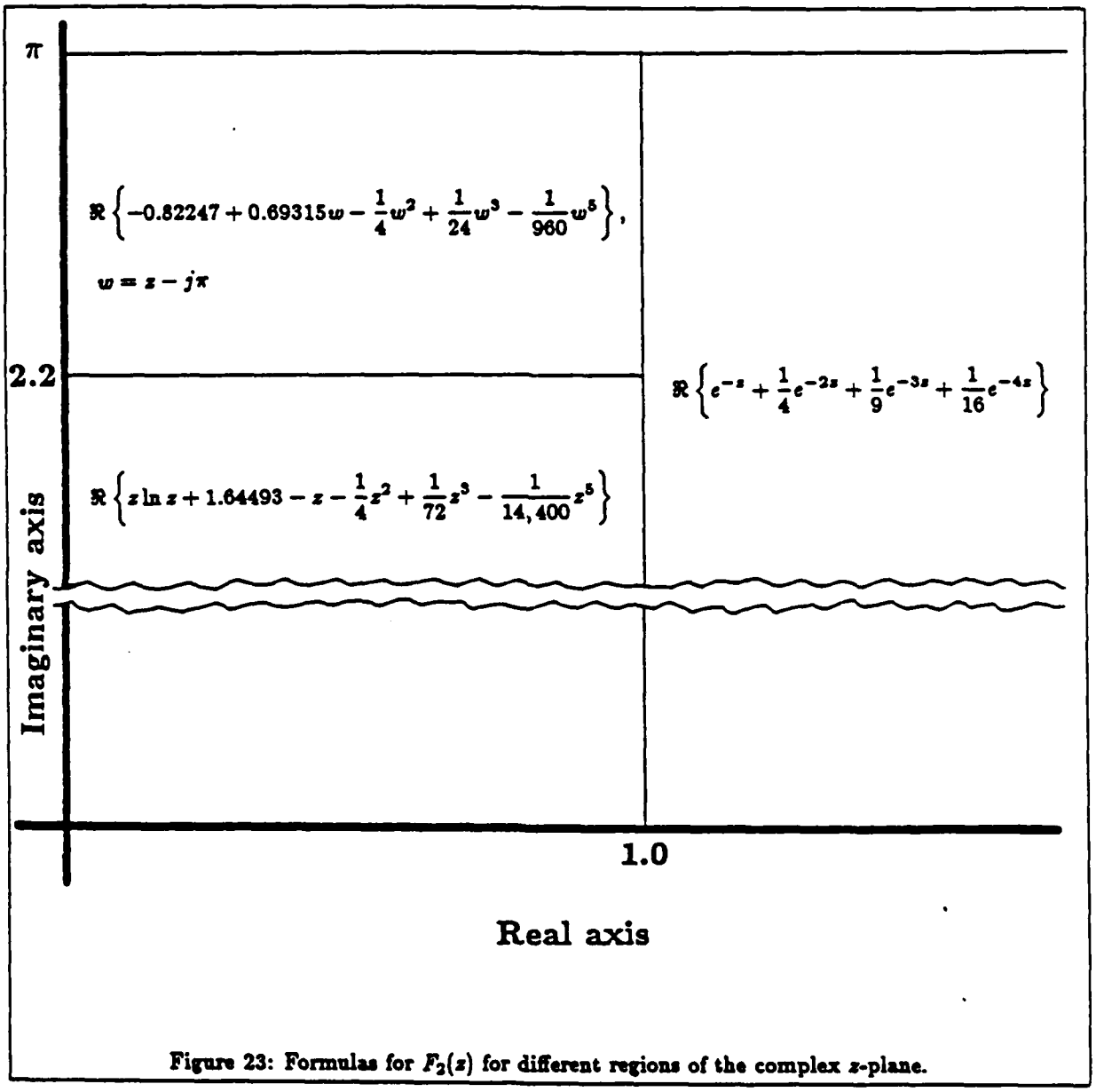

Figure 23: Formulas for $F_2(z)$ for different regions of the complex z-plane.

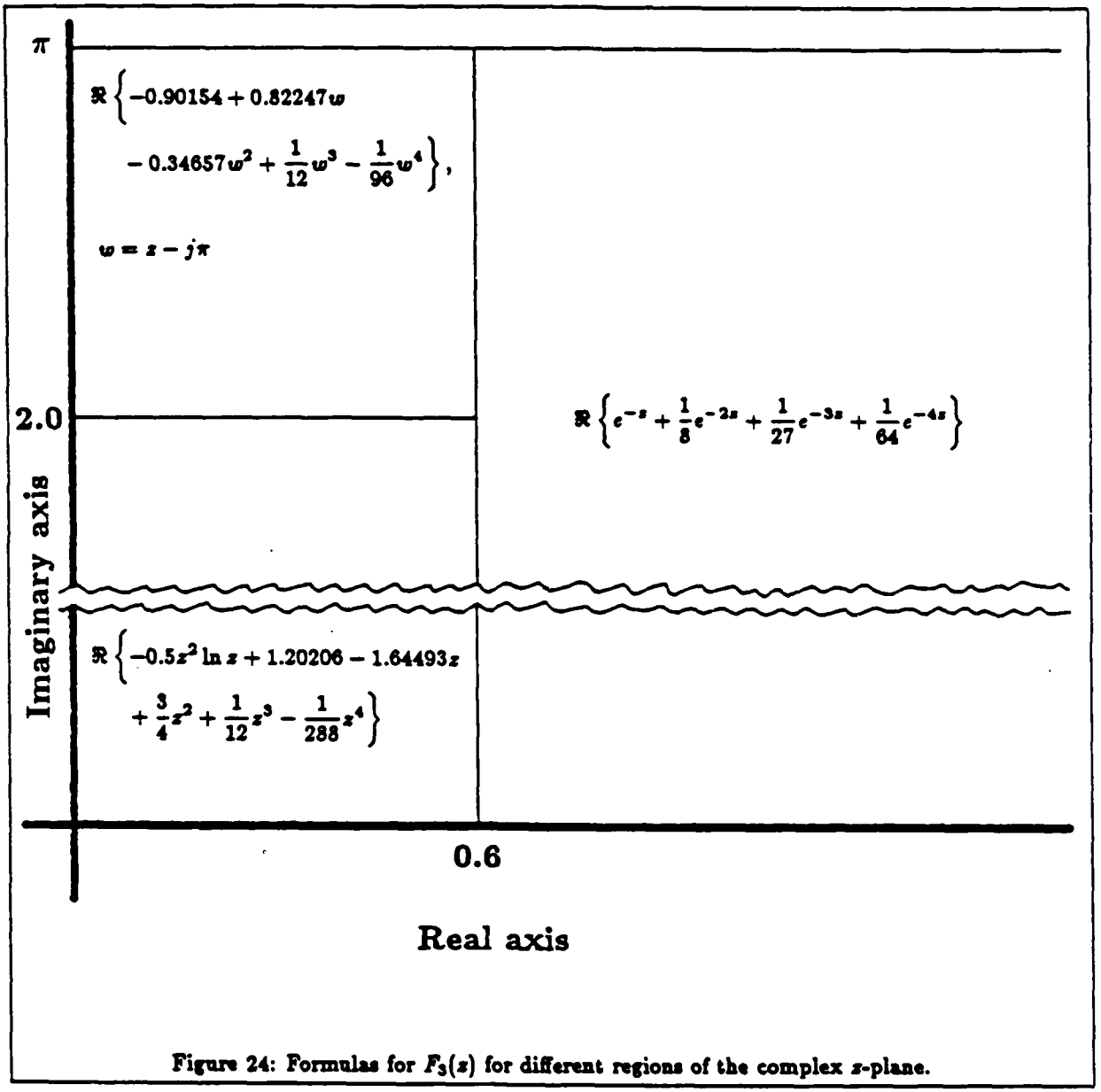

Figure 24: Formulas for $F_3(z)$ for different regions of the complex z-plane.

$$F_n(z) = F_n(z \bmod 2\pi),$$

$$F_n(z) = F_n(z^*).$$

This method has been used to obtain explicit formulas for the several differently shaped patches. The formulas for rectangular patches are

$$\begin{aligned}
z_0 &= \frac{\pi}{a}[(y_> - y_<) + j(x - x')], \\
z_1 &= \frac{\pi}{a}[(y_> + y_<) + j(x - x')], \\
z_2 &= \frac{\pi}{a}\{[2b - (y_> + y_<)] + j(x - x')\}, \\
z_3 &= \frac{\pi}{a}[(y_> - y_<) + j(x + x')], \\
z_4 &= \frac{\pi}{a}[(y_> + y_<) + j(x + x')], \\
z_5 &= \frac{\pi}{a}\{[2b - (y_> + y_<)] + j(x + x')\}, \\
r_{00} &= \frac{1}{2S}\left\{\frac{b^2}{3} - [y_<^2 + (b - y_>)^2]\right\}, \\
r_{10} &= \frac{1}{4S}\left\{\frac{1}{6}[y_<^2 + (b - y_>)^2] + y_<^2(b - y_>)^2 - \frac{1}{3}b^2[y_<^2 + (b - y_>)^2] + \frac{7}{90}b^2\right\}, \\
\sigma_\ell &= -\Re\{z_\ell\}, \quad \ell = 0, 1, 2, \\
\sigma_4 &= -\frac{\pi}{a}[2b - (y_> - y_<)],
\end{aligned}$$

$$\begin{aligned}
\Omega_{0m}(y|y') &= \frac{\sum_{\ell=0}^{3} e^{m\sigma_\ell}}{1 - e^{-2m\pi b/a}}, \\
\Omega_{1m}(y|y') &= \frac{\sum_{\ell=0}^{3} (b\pi/a + \sigma_\ell) e^{m\sigma_\ell}}{1 - e^{-2m\pi b/a}}, \\
\Omega_{2m}(y|y') &= \left[\frac{1}{m} + \frac{b\pi}{a}\coth(m\pi b/a)\right]\Omega_{0m}(y|y') - \Omega_{1m}(y|y'),
\end{aligned}$$

$$H_1(z) = \begin{cases} F_1(z), & |z| \geq \dfrac{\pi d}{2a}; \\ F_1\left(\dfrac{\pi d}{2a}\right), & |z| < \dfrac{\pi d}{2a}, \end{cases}$$

$$G_0(r|r') = r_{00} - \frac{1}{\pi}\left\{\sum_{m=1}^{\infty}\frac{1}{m}\left[\Omega_{0m}(y|y') - \sum_{\ell=0}^{2} e^{m\sigma_\ell}\right]\cos\left(\frac{m\pi x}{a}\right)\cos\left(\frac{m\pi x'}{a}\right) - \frac{1}{2}\sum_{\ell=0}^{5} H_1(z_\ell)\right\},$$

$$G_1(r|r') = r_{10} - \frac{a^2}{2\pi^3}\left\{\sum_{m=1}^{\infty}\frac{1}{m^2}\left[\Omega_{2m}(y|y') - \sum_{\ell=0}^{2}\left(\frac{1}{m}-\sigma_\ell\right)e^{m\sigma_\ell}\right]\cos\left(\frac{m\pi x}{a}\right)\cos\left(\frac{m\pi x'}{a}\right) - \frac{1}{2}\sum_{\ell=0}^{5}[F_3(z_\ell) - \sigma_\ell F_2(z_\ell)]\right\}.$$

These series typically do not require more than two or three terms for adequate convergence.

A.2 Computation of the Far-Field Pattern

Given a patch with a set of L sample points (u_ℓ, v_ℓ) along its edge (with $(u_L, v_L) = (u_1, v_1)$), where (u, v) is a point in the curvilinear coordinate system used to describe the patch, one can compute the approximate far-field in the following way. First, sample the loaded element mode $\Psi(u, v)$ at each of the sample points thus forming the set

$$\Psi^{(\ell)} = \Psi(u_\ell, v_\ell).$$

Then the far-field components of the electric field are given by the following formulas.

$$E_\theta = jk_0 t(F_x \sin\phi - F_y \cos\phi)\frac{1}{4\pi r}e^{-jk_0 r},$$

$$E_\phi = jk_0 t(F_x \cos\phi + F_y \sin\phi)\cos\theta\frac{1}{4\pi r}e^{-jk_0 r},$$

where

$$F = \sum_{\ell=0}^{L}\hat{\tau}_\ell\left[\overline{\Psi}^{(\ell)} j_0\left(\frac{1}{2}k_0\hat{r}\cdot\Delta r_\ell\right) + j\frac{\Delta\Psi^{(\ell)}}{2} j_1\left(\frac{1}{2}k_0\hat{r}\cdot\Delta r_\ell\right)\right]\Delta s_\ell e^{jk_0\hat{r}\cdot\overline{r}_\ell},$$

$$\overline{\Psi}^{(\ell)} = \frac{1}{2}\left[\Psi(u_{\ell+1}, v_{\ell+1}) + \Psi(u_\ell, v_\ell)\right],$$

$$\Delta\Psi^{(\ell)} = \Psi(u_{\ell+1}, v_{\ell+1}) - \Psi(u_\ell, v_\ell),$$

$$r_\ell = x_\ell\hat{x} + y_\ell\hat{y}, \qquad \overline{r}_\ell = \frac{1}{2}(r_{\ell+1} + r_\ell), \qquad \Delta r_\ell = r_{\ell+1} - r_\ell,$$

$$u_\ell = u(x_\ell, y_\ell), \qquad v_\ell = v(x_\ell, y_\ell), \qquad \Delta s_\ell = |\Delta r_\ell|, \qquad \hat{\tau}_\ell = \frac{\Delta r_\ell}{\Delta s_\ell},$$

$$\hat{r} = \hat{x}\cos\phi\sin\theta + \hat{y}\sin\phi\sin\theta + \hat{z}\cos\theta,$$

$$j_0(x) = \frac{\sin x}{x}, \qquad j_1(x) = \frac{\sin x}{x^2} - \frac{\cos x}{x}.$$

A.3 The Computation of the Energy Stored in the Cavity

This section deals with the efficient computation of the electric stored energy within a microstrip antenna loaded with N lumped, linear loads. The expression for the loaded mode distribution is given in equation (3) in Section 2. The actual load currents, which are distributed over a finite area, are assumed to be filamentary for the purpose of computing energy. This can be done because while the field itself arising under this assumption has log singularity, the square of this field over the volume of the cavity is integrable. The associated stored energy times ω is given by equation (4) Section 2. This series converges slowly enough that some moderate acceleration is useful. The series is summed, approximately, by extracting a single quasi-static term. This quasi-static term is identical to the 1^{st}-order quasi-static term of the expansion of the Green's function itself.

The ratio

$$\frac{1}{(k^2 - k_{mn}^2)^2} \approx b_0 \frac{1}{k_{mn}^4} + b_1 \frac{k^2}{k_{mn}^6} \tag{10}$$

for $(m,n) \in A_\xi$. The set A_ξ is the same as that defined in Section A.1. For the sake of numerical efficiency, the same value of ξ should be used in this computation as that used for computing the field in equation (6) of Section A.1. Using the approximation in (10), one arrives at

$$\begin{aligned} W_E &= \frac{1}{2} t \epsilon_r \mu_r^2 k_0^3 \eta_0 \sum_{\ell=0}^{N} \sum_{i=0}^{N} I_\ell I_i \\ &\quad \cdot \left\{ \frac{1}{Sk^4} + \sum_{\overline{A}_\xi} \left(\frac{1}{(k^2 - k_{mn}^2)^2} - b_0 \frac{1}{k_{mn}^2} - b_1 \frac{k^2}{k_{mn}^4} \right) \psi_{mn}(\boldsymbol{r}_i) \psi_{mn}(\boldsymbol{r}_\ell) \right. \\ &\quad \left. - b_0 G_1(\boldsymbol{r}_i | \boldsymbol{r}_\ell) - b_1 k^2 G_2(\boldsymbol{r}_i | \boldsymbol{r}_\ell) \right\}, \end{aligned}$$

where

$$G_2(\boldsymbol{r}|\boldsymbol{r}') = -\sum_{A_0} \frac{\psi_{mn}(\boldsymbol{r}) \psi_{mn}(\boldsymbol{r}')}{k_{mn}^6}.$$

The computation of $G_1(\boldsymbol{r}|\boldsymbol{r}')$ is discussed in Section A.1. The computation of $G_2(\boldsymbol{r}|\boldsymbol{r}')$ could be handled in the same way as the computation of the lower-order quasistatic terms, but this is too tedious a computation. Instead, $G_2(\boldsymbol{r}|\boldsymbol{r}')$ is summed directly.

The coefficients b_0 and b_1 are the solution of the minimax problem,

$$\min_{b_0, b_1} \left\{ \max_{0 \le x \le 1/\xi^2} |\eta(x)| \right\},$$

where

$$\eta(x) = \frac{1}{(1-x)^2} - b_0 - b_1 x$$

A plot of $\eta(x)$ *versus* x will show that the minimax solution will satisfy

$$\eta(0) = \eta(1/\xi^2)$$

and

$$\eta(0) = -\eta(x_{\max}),$$

where $x_{\max}$ satisfies

$$\frac{d}{dx}\eta(x) = \frac{2}{(1-x)^3} - b_1 = 0.$$

The solution to this is

$$x_{\max} = 1 - \left(\frac{2}{b_1}\right)^{1/3}.$$

The solution to the minimax problem is

$$b_1 = \left(\frac{1}{(1-1/\xi^2)^2 - 1}\right)\xi^2$$

$$b_0 = \frac{1}{2}\left(1 - b_1 + 3\left(\frac{b_1}{2}\right)^{2/3}\right).$$

For $\xi = 2$, these parameters are

$$b_0 = 0.958$$

and

$$b_1 = 3.111.$$

This approximation yields a maximum error of about 4%.

The next problem is to find $G_2(\mathbf{r}|\mathbf{r}')$. What is the error if $G_2(\mathbf{r}|\mathbf{r}')$ were only summed over $\overline{A}_\xi$? If $\xi = 2$, then a *typical* relative error level would be *no worse* than

$$2^{-4} \approx 0.06.$$

This is because $k_{\max}$ is typically greater than or equal to the smallest *non-zero* k_{mn}. Contributions to the sum outside of $\overline{A}_\xi$ are at least 2^{-6} times as small as the contribution due to the smallest k_{mn}. In the worst case, all contributions outside of $\overline{A}_\xi$ add in phase (when the source and observation points coincide) in which case the sum can be approximated by a continuous integral over wavenumber. This accounts for the exponent of 4 in the previous equation. This approximation of truncating $G_2(\mathbf{r}|\mathbf{r}')$ to just a sum over $\overline{A}_\xi$ should be adequate. Under this approximation, the expression for W_E becomes

$$W_E = \frac{1}{2}t\epsilon_r\mu_r^2 k_0^3\eta_0 \sum_{\ell=0}^{N}\sum_{i=0}^{N} I_\ell I_i \left\{\frac{1}{Sk^4} + \sum_{\overline{A}_\xi}\left(\frac{1}{(k^2 - k_{mn}^2)^2} - b_0\frac{1}{k_{mn}^4}\right)\psi_{mn}(\mathbf{r}_i)\psi_{mn}(\mathbf{r}_\ell) - b_0 G_1(\mathbf{r}_i|\mathbf{r}_\ell)\right\}.$$

MISSION
of
Rome Air Development Center

RADC plans and executes research, development, test and selected acquisition programs in support of Command, Control, Communications and Intelligence (C^3I) activities. Technical and engineering support within areas of competence is provided to ESD Program Offices (POs) and other ESD elements to perform effective acquisition of C^3I systems. The areas of technical competence include communications, command and control, battle management, information processing, surveillance sensors, intelligence data collection and handling, solid state sciences, electromagnetics, and propagation, and electronic, maintainability, and compatibility.

END

6-87

DTIC